A priori and a posteriori analyses of a quasi-static fractional order viscoelasticity model

Yongseok Jang

A priori and a posteriori analyses of a quasi-static fractional order viscoelasticity model

A PREPRINT

Yongseok Jang

LIP6, Sorbonne University, Paris, France. Email: yongseok.jang@lip6.fr.

October 23, 2024

ABSTRACT

A power-law type stress relaxation leads to a fractional order viscoelasticity model. We consider the quasi-static fractional order viscoelasticity model which is mathematically expressed as a Volterra integral of the second kind with a weakly singular kernel. Employing the *symmetric interior penalty discontinuous Galerkin* (SIPG) method and linear interpolation in time, we derive the fully discrete problem. To mitigate temporal discretization errors from a physical perspective in the quasi-static state, we introduce an auxiliary discrete velocity using the Crank-Nicolson approximation. We present *a priori* stability and error analyses for both the semi-discrete and fully discrete schemes. Additionally, we provide a residual-based *a posteriori* energy error estimation. Finally, we conduct numerical experiments that validate the error estimate theorems and demonstrate their applicability using real material data.

Keywords: Quasi-static fractional order viscoelasticity; Symmetric interior penalty discontinuous Galerkin method; *A priori* analysis; *A posteriori* analysis

MSC: 45D05, 65M12, 74D05, 74S05

1 Introduction

Viscoelasticity is a crucial characteristic observed in a diverse array of materials, such as polymers, gels, biological tissues, and certain metals, as demonstrated in [1, 2, 3]. This unique property enables materials to exhibit a combination of elastic and viscous behavior. In contrast to purely elastic materials, which deform instantaneously and fully return to their original shape upon the removal of applied loads, viscoelastic materials exhibit time-dependent deformations and energy dissipation during both loading and unloading phases. To effectively describe the viscoelastic behavior of these materials, several models have been developed, including the Maxwell, Kelvin-Voigt, and Zener models. These rheological frameworks utilize various configurations of springs and dashpots to represent the elastic and viscous components of the materials, thereby providing a robust foundation for capturing the complex viscoelastic responses. For a comprehensive exploration of these models and their applications, we refer readers to the literature, e.g., [4, 5, 6] and the references therein.

In this paper, we focus specifically on a power-law type constitutive model, motivated by the intermediate behavior observed between elastic solids and viscous liquids in continuum mechanics. In this framework, the stress $\underline{\boldsymbol{\sigma}}$ is proportional to the strain $\underline{\boldsymbol{\varepsilon}}$ in solids, represented as $\underline{\boldsymbol{\sigma}} \propto \underline{\boldsymbol{\varepsilon}}$, while in a Newtonian fluid, the stress is proportional to the rate of strain, expressed as $\underline{\boldsymbol{\sigma}} \propto \dot{\underline{\boldsymbol{\varepsilon}}}$. Therefore, the power-law constitutive law can be formulated as $\underline{\boldsymbol{\sigma}} \propto \partial_t^\alpha \underline{\boldsymbol{\varepsilon}}$, where ∂_t^α denotes a fractional order time differential operator of order α, with $0 < \alpha < 1$. For instance, in the study by Torvik and Bagley [7], the constitutive relationship for the elastomer 3M-467 is characterized by $\underline{\boldsymbol{\sigma}} \propto \partial_t^{0.56} \underline{\boldsymbol{\varepsilon}}$. This highlights the relevance of fractional derivatives in modeling the stress-strain behavior of viscoelastic materials. By exploring the implications of such models, we can better understand the time-dependent mechanical responses of viscoelastic materials, paving the way for improved applications in various fields, including material design and structural analysis.

McLean and Thomée [8, 9, 10] developed numerical analysis techniques specifically for fractional order evolution equations, particularly in relation to scalar analogues of power-law type viscoelasticity problems. Their investigations focused primarily

on error analysis under homogeneous Dirichlet boundary conditions, offering valuable insights into the numerical aspects of fractional order evolution problems. However, their analyses are constrained by the reliance on spectral methods, which limit applicability to purely homogeneous Dirichlet conditions. On the other hand, recent studies by Jang and Shaw[11, 12] have addressed the well-posedness and error estimates of vector-valued fractional order dynamic viscoelasticity problems with mixed boundary conditions. These works utilized duality arguments and an L_∞ approach in time, avoiding reliance on Grönwall's inequality and spectral methods. Another fractional order viscoelasticity problem such as Mittag-Leffler type, has been conducted in [13, 14, 15].

The quasi-static state of fractional order viscoelasticity is particularly significant for understanding material if the inertial forces resulting from the deformation are small. Unlike dynamic problems, where inertial effects and rapid loading rates dominate, the quasi-static framework allows for a more focused analysis of viscoelastic responses without the complexities introduced by inertia. This approach is essential in applications across civil engineering, biomechanics, and materials science, where materials often endure gradual changes in load over time. Focusing on this model enables the development of robust numerical methods that enhance predictive capabilities and facilitate better material selection and engineering design in real-world applications. We refer to early works of Simon and Whiteman [16, 17] for the numerical analysis of quasi-static hereditary linear viscoelasticity problems. For *a posteriori* analyses of elasticity and viscoelasticity problems, we also refer to [17, 18, 19] and [20, 21], respectively.

In this paper, we approximate the quasi-static fractional order viscoelasticity model of a power-law type using the *discontinuous Galerkin finite element method* (DGFEM), specifically the *symmetric interior penalty Galerkin method* (SIPG) for spatial discretization. The presence of a weak singularity in the fractional order Volterra kernel requires special treatment to maintain both accuracy and stability. Typical numerical approaches, such as standard quadrature rules developed for integer-order integral equations, may not be suitable and may suffer from a loss of accuracy when applied to fractional order problems. To address these challenges, we employ linear interpolation techniques [22] to manage the weak singularity in the numerical scheme. Also, the temporal error can be reduced by introducing the discrete velocity with Crank-Nicolson type finite difference scheme, otherwise it holds $1 + \alpha$ accuracy in time [23, 24]. We establish stability bounds and spatially optimal error estimates for the discrete problems providing optimal spatial orders of convergence and second order accuracy in time. Furthermore, we present a residual-based *a posteriori* error estimation of the semi-discrete problem. Due to the fundamental characteristics of the quasi-static state, the error estimator is also applicable to the fully discrete scheme in practice.

To our knowledge, this work is the first to provide both *a priori* and *a posteriori* error analyses for the symmetric interior penalty Galerkin (SIPG) method applied to the quasi-static viscoelasticity model of power-law type with mixed boundary conditions. Previous studies in this area often made additional assumptions, such as enforcing completely a homogeneous Dirichlet boundary condition and considering different model problems including those with exponentially decaying kernels [16, 17] and Mittag-Leffler types [25, 18, 14]. The numerical simulation of the Mittag-Leffler type model tends to be more computationally intensive because they require handling infinite series. Furthermore, the numerical methods outlined in [18, 14] only achieve first-order temporal accuracy, and [15] demonstrates optimal spatial error estimates using Grönwall's inequality without a thorough temporal error assessment. Consequently, the contribution of our research is to enhance the understanding of *a priori* and *a posteriori* error estimations for more generalized quasi-static fractional order viscoelasticity problems.

The structure of this paper is as follows. In Section 2, we introduce the notation, the framework of the DGFEM, and the essential definitions of fractional calculus. Section 3 presents the quasi-static fractional order viscoelasticity model, defining both a semi-discrete and a fully discrete formulation. The stability analysis and *a priori* error bounds are established and proved in Section 4. An *a posteriori* error analysis is conducted in Section 5. Section 6 showcases numerical experiments performed using FEniCS (`https://fenicsproject.org/`). Finally, Section 7 provides concluding remarks on the findings of the study.

2 Preliminary

We use standard notation; $L_p(\Omega)$, $H^s(\Omega)$ and $W_p^s(\Omega)$ with non-negative s and p, denoting the usual Lebesgue, Hilbert, and Sobolev spaces, respectively. For a normed space X, $\|\cdot\|_X$ represents the norm in the space X. In inner product spaces, this norm is always the one induced by the inner product. For example, $\|\cdot\|_{L_2(\Omega)}$ is the $L_2(\Omega)$ norm, as induced by the $L_2(\Omega)$ inner product, which we denote simply $(\cdot,\cdot)$ for brevity. However, for any $S \subset \bar{\Omega}$, we use $(\cdot,\cdot)_{L_2(S)}$ to indicate the $L_2(S)$ inner product. When we refer to the Bochner space by $L_p(0,T;X)$, for a time-dependent function $f \in L_p(0,T;X)$, the corresponding norm is defined by

$$\|f\|_{L_p(0,T;X)} = \left(\int_0^T \|f(t)\|_X^p \, dt\right)^{1/p},$$

for $1 \le p < \infty$. When $p = \infty$ this is known as the *essential supremum* norm:

$$\|f\|_{L_\infty(0,T;X)} = \operatorname*{ess\,sup}_{0\le t\le T} \|f(t)\|_X.$$

When convenient, we may replace the upper limit T in these expressions with another value e.g., $t \in [0, T]$ and we denote a time derivative by overdot, for example,

$$\dot{f}(t) = \frac{\partial f}{\partial t}.$$

We use the same notation for inner products of vector-valued and tensor-valued functions as in the scalar case. For instance, we have

$$(\boldsymbol{v}, \boldsymbol{w}) = \int_\Omega \boldsymbol{v} \cdot \boldsymbol{w}\, d\Omega, \qquad (\underline{\boldsymbol{v}}, \underline{\boldsymbol{w}}) = \int_\Omega \underline{\boldsymbol{v}} : \underline{\boldsymbol{w}}\, d\Omega = \sum_{i,j=1}^{d} \int_\Omega v_{ij} w_{ij}\, d\Omega,$$

where $\boldsymbol{v}$ and $\boldsymbol{w}$ are vector-valued functions, and $\underline{\boldsymbol{v}}$ and $\underline{\boldsymbol{w}}$ are second order tensors. Also, we use the outer product $\otimes$ such that for vectors $\boldsymbol{a}$ and $\boldsymbol{b}$, $(\boldsymbol{a} \otimes \boldsymbol{b})_{mn} = a_m b_n$ for $m, n = 1, \ldots, d$.

2.1 Finite element space

Following the DGFEM framework from [26], we subdivide the domain $\Omega \subset \mathbb{R}^d$ into elements $E \in \mathcal{E}_h$ (triangles in 2D or tetrahedrons in 3D). The mesh is assumed to be shape regular and quasi-uniform with $h \leq C h_E$ where h_E is the diameter of E and h is the maximum diameter. We denote the set of interior edges/faces e as Γ_h, with unit normal vectors $\boldsymbol{n}_e$ defined for each element.

The broken Sobolev space is given by

$$H^s(\mathcal{E}_h) = \left\{ v \in L_2(\Omega) \mid \forall E \in \mathcal{E}_h,\ v|_E \in H^s(E) \right\}$$

with the broken Sobolev norm, $|||\cdot|||_{H^s(\mathcal{E}_h)}$, defined as

$$|||v|||_{H^s(\mathcal{E}_h)} = \left(\sum_{E \in \mathcal{E}_h} \|v\|^2_{H^s(E)} \right)^{1/2}.$$

This extends naturally to vector fields, and the DG finite element space $\boldsymbol{\mathcal{D}}_k(\mathcal{E}_h)$ is similarly defined using polynomials of degree k over each element. Hence we can derive the vector field analogue $\boldsymbol{\mathcal{D}}_k(\mathcal{E}_h) = [\mathcal{D}_k(\mathcal{E}_h)]^d$, where

$$\mathcal{D}_k(\mathcal{E}_h) = \left\{ v \in H^1(\mathcal{E}_h) \;\middle|\; v|_E \in \mathcal{P}_k(E) \text{ for each } E \in \mathcal{E}_h \right\},$$

and $\mathcal{P}_k(E)$ is the space of polynomials of degree less than or equal to k over E.

For a vector valued function $\boldsymbol{v}$, we define the average and jump on e shared by elements E_i and E_j (with the normal vector $\boldsymbol{n}_e$ from E_i to E_j):

$$\{\boldsymbol{v}\} = \left((\boldsymbol{v}|_{E_i})|_e + (\boldsymbol{v}|_{E_j})|_e \right)/2, \qquad [\boldsymbol{v}] = (\boldsymbol{v}|_{E_i})|_e - (\boldsymbol{v}|_{E_j})|_e,$$

and similarly for tensors. If $e \subset \partial\Omega$, we simplify these definitions using boundary values. Finally, we can introduce the jump penalty operator defined as

$$J_0^{\gamma_0, \gamma_1}(\boldsymbol{v}, \boldsymbol{w}) = \sum_{e \subset \Gamma_h \cup \Gamma_D} \frac{\gamma_0}{|e|^{\gamma_1}} \int_e [\boldsymbol{v}] \cdot [\boldsymbol{w}]\, de,$$

where γ_0 and γ_1 are positive constants.

Proposition 1 (Inverse polynomial trace inequalities[27])**.** *For any $v \in \mathcal{P}_k(E)$, $\forall e \subset \partial E$,*

$$\begin{cases} \|v\|_{L_2(e)} & \leq C|e|^{1/2}|E|^{-1/2}\|v\|_{L_2(E)}, \\ \|v\|_{L_2(e)} & \leq C h_E^{-1/2}\|v\|_{L_2(E)}, \\ \|\nabla v \cdot \boldsymbol{n}_e\|_{L_2(e)} & \leq C|e|^{1/2}|E|^{-1/2}\|\nabla v\|_{L_2(E)}, \\ \|\nabla v \cdot \boldsymbol{n}_e\|_{L_2(e)} & \leq C h_E^{-1/2}\|\nabla v\|_{L_2(E)}, \end{cases} \tag{2.1}$$

where C is a positive constant and is independent of h_E but depends on the polynomial degree k.

Proposition 2 (Poincaré's Inequality[28, 26])**.** *If $\gamma_1(d-1) \geq 1$ and $|e| \leq 1$ for every $e \subset \Gamma_h \cup \Gamma_D$, then there exists a positive constant C such that*

$$\|v\|_{L_2(\Omega)} \leq C \left(|||\nabla v|||^2_{H^0(\mathcal{E}_h)} + \sum_{e \subset \Gamma_h \cup \Gamma_D} \frac{1}{|e|^{\gamma_1}} \|[v]\|^2_{L_2(e)} \right)^{1/2}, \tag{2.2}$$

for any $v \in H^1(\mathcal{E}_h)$.

Proposition 3 (Inverse Inequality or Markov Inequality[29, 26]). *For any $E \in \mathcal{E}_h$, there is a positive constant C such that*

$$\forall v \in \mathcal{P}_k(E),\ \left\|\nabla^j v\right\|_{L_2(E)} \leq C h_E^{-j} \left\|v\right\|_{L_2(E)},\ \forall j \in \{0, 1, \ldots, k\}, \tag{2.3}$$

where

$$\nabla^j v = \begin{cases} \nabla \cdot \nabla^{j-1} v & \text{for even } j, \\ \nabla(\nabla^{j-1} v) & \text{for odd } j, \end{cases} \qquad \text{and} \qquad \nabla^0 v = v.$$

2.2 Fractional calculus

Here, we present the definition of the (left) Riemann-Liouville fractional derivative and its properties.

Definition 1 (Riemann-Liouville fractional derivative and integral). *Let f be a function defined on $[a, b]$ and $\alpha \in \mathbb{R}^+$ written uniquely as $\alpha = n_\alpha + q_\alpha$ for $n_\alpha \in \mathbb{N} \cup \{0\}$, $q_\alpha \in [0, 1)$. The left Riemann-Liouville derivative of order α is defined by*

$${}_aD_t^\alpha f(t) = \frac{1}{\Gamma(n-\alpha)} \left(\frac{d}{dt}\right)^n \int_a^t f(t')(t-t')^{n-\alpha-1} dt',\ t > a,$$

where $n = n_\alpha + 1$ and Γ is the gamma function. If $f \in L_1(a, b)$, we can define a left fractional integral of order α by

$${}_aI_t^\alpha f(t) = \frac{1}{\Gamma(\alpha)} \int_a^t f(t')(t-t')^{\alpha-1} dt',\ t > a.$$

For $\alpha \in (0, 1)$, we can observe that

$${}_aD_t^\alpha f(t) = \frac{d}{dt}\, {}_aI_t^{1-\alpha} f(t), \qquad \text{and} \qquad {}_aD_t^\alpha f(t) = \frac{f(a)(t-a)^{-\alpha}}{\Gamma(1-\alpha)} + {}_aI_t^{1-\alpha} \dot{f}(t).$$

Furthermore, we have the positive definiteness [8] of the fractional integral of order $\alpha \in (0, 1)$ such that

$$\int_0^T {}_0I_t^{1-\alpha} \phi(t)\phi(t) dt = \frac{1}{\Gamma(1-\alpha)} \int_0^T \int_0^t (t-t')^{-\alpha} \phi(t')\phi(t) dt' dt \geq 0. \tag{2.4}$$

Remark 1. *In addition to the Riemann-Liouville fractional calculus, other commonly used definitions include the Caputo [30] and Grunwald-Letnikov fractional derivatives [31, 32]. The Caputo derivative is often preferred in practical applications because it allows traditional initial and boundary conditions to be included in the formulation of the problem and its derivative of a constant is zero. The Grunwald-Letnikov derivative, on the other hand, is often seen as a more direct discretization of fractional derivatives, making it useful in numerical approximations. Nevertheless, in this paper, we focus solely on the Riemann-Liouville formulation due to its suitability for our problem setting and its analytical properties in fractional viscoelastic models.*

3 Model problem

We introduce a quasi-static viscoelasticity problem of the power-law type [33]. For the space discretization, we employ the SIPG method resulting in a semi-discrete formulation. Then, using linear interpolation [22], we obtain a numerical solution from the fully discrete problem.

According to the power-law type stress relaxation [33], the constitutive equation is defined as

$$\underline{\boldsymbol{\sigma}}(t) = \varphi_0 \underline{\boldsymbol{D}}\underline{\boldsymbol{\varepsilon}}(t) + \varphi_1 \Gamma(1-\alpha) {}_0I_t^{1-\alpha} \underline{\boldsymbol{D}}\dot{\underline{\boldsymbol{\varepsilon}}}(t), \tag{3.1}$$

where φ_0 is non-negative, φ_1 is positive and $\underline{\boldsymbol{D}}$ is a symmetric positive definite piecewise constant fourth-order tensor. For instance, using the Einstein's convention notation and the Kronecker delta, we define $\underline{\boldsymbol{D}}$ by

$$D_{ijkl} = 2\mu \delta_{ik}\delta_{jl} + \lambda \delta_{ij}\delta_{kl},$$

where μ and λ are interpreted as Lamé parameters. Unlike the dynamic viscoelastic problem [11, 12], the equilibrium condition of the quasi-static state leads us to obtain the following model problem:

$$-\nabla \cdot \underline{\boldsymbol{\sigma}}(t) = \boldsymbol{f}(t), \tag{3.2}$$

on $\Omega \times (0, T]$, and the substitution of (3.1) into (3.2) yields to

$$-\nabla \cdot \left(\varphi_0 \underline{\boldsymbol{D}}\underline{\boldsymbol{\varepsilon}}(t) + \varphi_{\alpha 0} I_t^{1-\alpha} \underline{\boldsymbol{D}}\dot{\underline{\boldsymbol{\varepsilon}}}(t)\right) = \boldsymbol{f}(t), \tag{3.3}$$

where $\varphi_\alpha := \varphi_1\Gamma(1-\alpha)$. Let $\boldsymbol{u}$ denote the displacement. The stress and strain are defined by $\underline{\boldsymbol{\sigma}}(t) = \underline{\boldsymbol{\sigma}}(\boldsymbol{u}(t))$ and $\underline{\boldsymbol{\varepsilon}}(t) = \underline{\boldsymbol{\varepsilon}}(\boldsymbol{u}(t))$, respectively, where we use the notation of Cauchy's infinitesimal tensor such that

$$\varepsilon_{ij}(\boldsymbol{v}) = \frac{1}{2}\left(\frac{\partial v_i}{\partial x_j} + \frac{\partial v_j}{\partial x_i}\right), \qquad \text{for } i,j = 1,\dots,d.$$

We suppose a mix of essential and natural boundary conditions so that

$$\boldsymbol{u}(t) = 0 \qquad \text{on } \Gamma_D \times [0,T], \qquad \text{and} \qquad \underline{\boldsymbol{\sigma}}(t)\cdot\boldsymbol{n} = \boldsymbol{g}_N(t) \text{on } \Gamma_N \times [0,T], \tag{3.4}$$

where Γ_D is the *Dirichlet* boundary (which is assumed to have positive surface measure), Γ_N is the *Neumann* boundary given by $\Gamma_N = \partial\Omega\backslash\Gamma_D$, $\boldsymbol{n}$ is the outward unit normal vector defined a.e. on Γ_N, and $\boldsymbol{g}_N$ prescribes surface traction on Γ_N. In addition, the initial conditions for the displacement and velocity are defined as follows:

$$\boldsymbol{u}(0) = \boldsymbol{u}_0 \qquad \text{and} \qquad \dot{\boldsymbol{u}}(0) = \boldsymbol{w}_0 \tag{3.5}$$

for given vector-fields $\boldsymbol{u}_0$ and $\boldsymbol{w}_0$.

3.1 Semi-discrete problem

Introducing the SIPG bilinear form in the context of our model problem, we present the semi-discrete formulation of the problem described in (3.3). We first define a symmetric DG bilinear form $a : \boldsymbol{H}^s(\mathcal{E}_h) \times \boldsymbol{H}^s(\mathcal{E}_h) \mapsto \mathbb{R}$ for $s > 3/2$ by

$$\begin{aligned} a(\boldsymbol{v},\boldsymbol{w}) = &\sum_{E\in\mathcal{E}_h}\int_E \underline{\boldsymbol{D}}\underline{\boldsymbol{\varepsilon}}(\boldsymbol{v}) : \underline{\boldsymbol{\varepsilon}}(\boldsymbol{w})\,dE - \sum_{e\subset\Gamma_h\cup\Gamma_D}\int_e \{\underline{\boldsymbol{D}}\underline{\boldsymbol{\varepsilon}}(\boldsymbol{v})\} : [\boldsymbol{w}\otimes\boldsymbol{n}_e]\,de \\ &- \sum_{e\subset\Gamma_h\cup\Gamma_D}\int_e \{\underline{\boldsymbol{D}}\underline{\boldsymbol{\varepsilon}}(\boldsymbol{w})\} : [\boldsymbol{v}\otimes\boldsymbol{n}_e]\,de + J_0^{\gamma_0,\gamma_1}(\boldsymbol{v},\boldsymbol{w}), \end{aligned} \tag{3.6}$$

for any $\boldsymbol{v},\boldsymbol{w} \in \boldsymbol{H}^s(\mathcal{E}_h)$. We also define our DG energy norm by

$$\|\boldsymbol{v}\|_V = \left(\sum_{E\in\mathcal{E}_h}\int_E \underline{\boldsymbol{D}}\underline{\boldsymbol{\varepsilon}}(\boldsymbol{v}) : \underline{\boldsymbol{\varepsilon}}(\boldsymbol{v})\,dE + J_0^{\gamma_0,\gamma_1}(\boldsymbol{v},\boldsymbol{v})\right)^{1/2}, \qquad \text{for } \boldsymbol{v} \in \boldsymbol{H}^s(\mathcal{E}_h).$$

In the DG bilinear form, the third term is called the "interior penalty" term, while the final term is known as the "jump penalty". The bilinear form can be either symmetric or nonsymmetric, depending on the sign of the interior penalty. In this paper, we focus on the symmetric DG method. For applications of the nonsymmetric approach to viscoelasticity, we refer to [34, 35].

Our choice of the SIPG method is driven by its efficiency. It requires only the standard penalization parameter $\gamma_1(d-1) \geq 1$ to achieve optimal spatial error estimates. In contrast, the nonsymmetric interior penalty Galerkin (NIPG) method demands a higher penalization parameter, $\gamma_1(d-1) \geq 3$, for similar error estimates. This higher penalization can result in a more ill-conditioned linear system, which may create challenges when using iterative solvers. For a more in-depth discussion of the nonsymmetric method, please see [34] and the references therein.

Following the standard DGFEM approach, we multiply equation (3.3) by a test function from the broken Sobolev space $\boldsymbol{H}^s(\mathcal{E}_h)$ for each $E \in \mathcal{E}_h$, integrate by parts over each element, sum across all elements, and introduce the necessary penalty terms. This process leads to the weak formulation of (3.3). Assuming the strong solution is spatially continuous, we incorporate the interior and jump penalty terms into our DG framework. This yields the following semi-discrete problem:
Find $\boldsymbol{u}_h : [0,T] \mapsto \boldsymbol{\mathcal{D}}_k(\mathcal{E}_h)$ satisfying for any $\boldsymbol{v} \in \boldsymbol{\mathcal{D}}_k(\mathcal{E}_h)$,

$$\varphi_0 a(\boldsymbol{u}_h(t),\boldsymbol{v}) + \varphi_\alpha a\left({}_0I_t^{1-\alpha}\dot{\boldsymbol{u}}_h(t),\boldsymbol{v}\right) = F(t;\boldsymbol{v}) \qquad \text{for } t > 0, \tag{3.7}$$

$$a(\boldsymbol{u}_h(0),\boldsymbol{v}) = a(\boldsymbol{u}_0,\boldsymbol{v}), \tag{3.8}$$

where the linear form $F(\cdot)$ is defined by

$$F(t;\boldsymbol{v}) = (\boldsymbol{f}(t),\boldsymbol{v}) + (\boldsymbol{g}_N(t),\boldsymbol{v})_{L_2(\Gamma_N)}.$$

Additionally, we can also impose the initial condition of velocity by

$$a(\dot{\boldsymbol{u}}_h(0),\boldsymbol{v}) = a(\boldsymbol{w}_0,\boldsymbol{v}). \tag{3.9}$$

It is straightforward to demonstrate that the linear form $F(\cdot)$ is continuous when $\boldsymbol{f} \in \boldsymbol{C}(0,T;\boldsymbol{L}_2(\Omega))$ and $\boldsymbol{g}_N \in \boldsymbol{C}(0,T;\boldsymbol{L}_2(\Gamma_N))$. Henceforth, we assume that the data terms are bounded and smooth enough to satisfy the continuity condition of the linear form with the initial condition $\boldsymbol{u}_0 \in \boldsymbol{H}^2(\Omega)\cap\boldsymbol{C}(\Omega)$. Also, when we suppose $\gamma_0 > 0$ is sufficiently large and

$\gamma_1(d-1) \geq 1$, the DG bilinear form $a(\cdot,\cdot)$ is coercive and continuous on $\boldsymbol{\mathcal{D}}_k(\mathcal{E}_h)$. Hence we have the positive constant κ and K such that

$$\kappa \|\boldsymbol{v}\|_V^2 \leq a(\boldsymbol{v},\boldsymbol{v}), \qquad \forall \boldsymbol{v} \in \boldsymbol{\mathcal{D}}_k(\mathcal{E}_h), \tag{3.10}$$

and

$$|a(\boldsymbol{v},\boldsymbol{w})| \leq K \|\boldsymbol{v}\|_V \|\boldsymbol{w}\|_V, \qquad \forall \boldsymbol{v},\boldsymbol{w} \in \boldsymbol{\mathcal{D}}_k(\mathcal{E}_h), \tag{3.11}$$

where κ and K are independent of $\boldsymbol{v}$ and $\boldsymbol{w}$, e.g., please see [34, 36] for more details.

We recall useful inequalities for *a priori* estimation theorems.

Proposition 4 (Korn's inequality for piecewise H^1 vector fields [26, 37])**.** *If we have $\gamma_1(d-1) \geq 1$, then since $\underline{\boldsymbol{D}}$ is symmetric positive definite and the jump penalty is defined not only on the interior edges but also on the positive measured Dirichlet boundary Γ_D, Korn's inequality yields, for any $\boldsymbol{v} \in \boldsymbol{H}^1(\mathcal{E}_h)$,*

$$\sum_{E\in\mathcal{E}_h} \|\nabla \boldsymbol{v}\|_{L_2(E)}^2 \leq C \|\boldsymbol{v}\|_V^2, \tag{3.12}$$

for some positive C independent of $\boldsymbol{v}$.

Proposition 5 (Bounds for interior penalty term [34, 36])**.** *Suppose $\gamma_0 > 0$ and $\gamma_1(d-1) \geq 1$. For any $\boldsymbol{v},\boldsymbol{w} \in \boldsymbol{\mathcal{D}}_k(\mathcal{E}_h)$, and for any pair $E_1, E_2 \in \mathcal{E}_h$, we have*

$$\begin{aligned}\left| \int_e \{\underline{\boldsymbol{D}}\underline{\boldsymbol{\varepsilon}}(\boldsymbol{v})\} : [\boldsymbol{w}\otimes\boldsymbol{n}_e]\, de \right| \leq & \frac{C}{\sqrt{\gamma_0}} \Big(\|\underline{\boldsymbol{D}}\underline{\boldsymbol{\varepsilon}}(\boldsymbol{v})\|_{L_2(E_1)}^2 + \|\underline{\boldsymbol{D}}\underline{\boldsymbol{\varepsilon}}(\boldsymbol{v})\|_{L_2(E_2)}^2 \\ & + \frac{\gamma_0}{|e|^{\gamma_1}} \|[\boldsymbol{w}]\|_{L_2(e)}^2 \Big), \end{aligned} \tag{3.13}$$

$$\sum_{e\subset\Gamma_h\cup\Gamma_D} \int_e \left| \{\underline{\boldsymbol{D}}\underline{\boldsymbol{\varepsilon}}(\boldsymbol{v})\} : [\boldsymbol{w}\otimes\boldsymbol{n}_e] \right| de \leq \frac{C}{\sqrt{\gamma_0}} \left(\|\boldsymbol{v}\|_V^2 + J_0^{\gamma_0,\gamma_1}(\boldsymbol{w},\boldsymbol{w}) \right), \tag{3.14}$$

where e is the shared edge of elements E_1 and E_2, and C is a positive constant independent of $\boldsymbol{v}$ and $\boldsymbol{w}$ but dependent on the inverse polynomial trace inequality's constants and the domain.

3.2 Temporal discretization

For the fully discrete formulation of the quasi-static viscoelastic model, we require numerical approximations for fractional order integration concerning the hereditary terms. In this study, we make use of the discrete time integrator defined by the linear interpolation technique [22, 11]. In addition, to approximate the velocity, we introduce an implicit temporal discretization of the Crank-Nicolson type.

Let $\Delta t = T/N > 0$ be a time step size for some $N \in \mathbb{N}$. The linear interpolation leads us to define a local interpolation operator $\mathcal{L}_n$ by

$$\mathcal{L}_n(\boldsymbol{w})(t) = -\frac{t-t_n}{\Delta t}\boldsymbol{w}(t_{n-1}) + \frac{t-t_{n-1}}{\Delta t}\boldsymbol{w}(t_n) \qquad \text{for } n = 1,\dots,N.$$

Using this local interpolation, we can derive a global piecewise linear interpolation of $\boldsymbol{w}$. We denote the local truncation error by $\boldsymbol{E}_n(t) = \boldsymbol{w}(t) - \mathcal{L}_n(\boldsymbol{w})(t)$. If $\boldsymbol{w}$ is of C^2 in time, Rolle's theorem implies that

$$\boldsymbol{E}_n(t) = \frac{1}{2}\ddot{\boldsymbol{w}}(\xi_t)(t-t_{n-1})(t-t_n) \qquad \text{for some } \xi_t \in [t_{n-1},t_n],$$

where $t \in [t_{n-1},t_n]$, and it satisfies that

$$\|\boldsymbol{E}_n(t)\|_X \leq \frac{\Delta t^2}{2} \|\ddot{\boldsymbol{w}}\|_{L_\infty(t_{n-1},t_n;X))},$$

when $\boldsymbol{w}(t) \in \boldsymbol{X}$ for a normed space $\boldsymbol{X}$. This inequality also holds on the broken Sobolev norm sense. Using the local interpolation operator and the local truncation error, we can define the numerical quadrature for fractional integral $\boldsymbol{q}_n(\boldsymbol{w})$ by

$$\begin{aligned} {}_0I_t^{1-\alpha}\boldsymbol{w}(t_n) =& \frac{1}{\Gamma(1-\alpha)} \sum_{i=1}^n \int_{t_{i-1}}^{t_i} \left(\mathcal{L}_i(\boldsymbol{w})(t') + \boldsymbol{E}_i(t')\right)(t_n-t')^{-\alpha} dt', \\ =& \frac{\Delta t^{1-\alpha}}{\Gamma(3-\alpha)} \sum_{i=0}^n B_{n,i}\boldsymbol{w}(t_i) + \frac{1}{\Gamma(1-\alpha)} \sum_{i=1}^n \int_{t_{i-1}}^{t_i} \boldsymbol{E}_i(t')(t_n-t')^{-\alpha} dt', \end{aligned}$$

$$:=\boldsymbol{q}_n(\boldsymbol{w})+\boldsymbol{e}_n(\boldsymbol{w}), \tag{3.15}$$

where

$$B_{n,i}=\begin{cases} n^{1-\alpha}(2-\alpha-n)+(n-1)^{2-\alpha}, & i=0,\\ (n-i-1)^{2-\alpha}+(n-i+1)^{2-\alpha}-2(n-i)^{2-\alpha}, & i=1,\dots,n-1,\\ 1, & i=n. \end{cases}$$

If $\boldsymbol{w}\in\boldsymbol{C}^2(0,T;X)$, the quadrature error is bounded by, for any $n=1,\dots,N$,

$$\|\boldsymbol{e}_n(\boldsymbol{w})\|_X=\|{}_0I_t^{1-\alpha}\boldsymbol{w}(t_n)-\boldsymbol{q}_n(\boldsymbol{w})\|_X\leq\frac{\Delta t^2}{2\Gamma(1-\alpha)}\|\ddot{\boldsymbol{w}}\|_{L_\infty(0,T;X)}T^{1-\alpha}. \tag{3.16}$$

For more details of the linear interpolation technique for fractional integral, we refer to [22, 34, 11] and the references therein.

We denote the fully discrete solutions for displacement and velocity by $\boldsymbol{U}_h^n\in\boldsymbol{\mathcal{D}}_k(\mathcal{E}_h)$ and $\boldsymbol{W}_h^n\in\boldsymbol{\mathcal{D}}_k(\mathcal{E}_h)$, respectively, for each time step $n=0,\dots,N$. Hence, $\dot{\boldsymbol{u}}(t_n)$ is approximated by $\boldsymbol{W}_h^n$ and $\boldsymbol{u}(t_n)$ is approximated by $\boldsymbol{U}_h^n$. To employ an implicit time integration, we additionally impose that

$$\frac{\boldsymbol{W}_h^{n+1}+\boldsymbol{W}_h^n}{2}=\frac{\boldsymbol{U}_h^{n+1}-\boldsymbol{U}_h^n}{\Delta t}. \tag{3.17}$$

Using the notation of discrete solutions, we denote the numerical fractional integration of velocity by

$$\boldsymbol{Q}_n(\boldsymbol{W}_h)=\frac{\Delta t^{1-\alpha}}{\Gamma(3-\alpha)}\sum_{i=0}^{n}B_{n,i}\boldsymbol{W}_h^i.$$

To derive the fully discrete formulation, we first suppose that $\boldsymbol{w}_0$ is the initial condition of velocity in $\boldsymbol{H}^2(\Omega)$. Then the fully discrete problem follows:
Find $\boldsymbol{W}_h^n\in\boldsymbol{\mathcal{D}}_k(\mathcal{E}_h)$ and $\boldsymbol{U}_h^n\in\boldsymbol{\mathcal{D}}_k(\mathcal{E}_h)$ for $n=0,\dots,N$ such that for any $\boldsymbol{v}\in\boldsymbol{\mathcal{D}}_k(\mathcal{E}_h)$,

$$\varphi_0 a\left(\frac{\boldsymbol{U}_h^{n+1}+\boldsymbol{U}_h^n}{2},\boldsymbol{v}\right)+\varphi_\alpha a\left(\frac{\boldsymbol{Q}_{n+1}(\boldsymbol{W}_h)+\boldsymbol{Q}_n(\boldsymbol{W}_h)}{2},\boldsymbol{v}\right)=\frac{1}{2}\left(F(t_{n+1};v)+F(t_n;v)\right), \tag{3.18}$$

for $n=0,\dots,N-1$, and

$$a\left(\boldsymbol{U}_h^0,\boldsymbol{v}\right)=a\left(\boldsymbol{u}_0,\boldsymbol{v}\right),\qquad\text{and}\qquad a\left(\boldsymbol{W}_h^0,\boldsymbol{v}\right)=a\left(\boldsymbol{w}_0,\boldsymbol{v}\right). \tag{3.19}$$

In (3.18), the numerical scheme includes the discrete velocity term $\boldsymbol{W}_h^n$. Indeed, the discrete velocity is an auxiliary variable to improve the accuracy of approximate velocity. Using the Crank-Nicolson relation (3.17), we can replace the discrete velocity terms with the linear combination of $(\boldsymbol{U}_h^i)_{i=1}^n$ and $\boldsymbol{W}_h^0$. In other words, we can write

$$\frac{\boldsymbol{Q}_{n+1}(\boldsymbol{W}_h)+\boldsymbol{Q}_n(\boldsymbol{W}_h)}{2}=\bar{c}_{n+1,0}\boldsymbol{W}_h^0+\sum_{i=0}^{n+1}c_{n+1,i}\boldsymbol{U}_h^i, \tag{3.20}$$

for some $\bar{c}_{n+1,0}$, $c_{n+1,0},\dots,c_{n+1,n+1}$. Nevertheless, for simple and clear notation in our proofs, we continue to use (3.18) with the discrete velocity term.

Remark 2. *In the work of Yan et al. [23], the linear interpolation without the presence of the auxiliary velocity, provides $1+\alpha$ order of accuracy. Please see also [24]. However, in our numerical scheme, the Crank-Nicolson approximation for velocity will lead to higher order of accuracy.*

4 A priori analysis

In this section, we prove *a priori* stability and error bounds. We consider the stability analyses of the semi-discrete problem and the fully discrete problem. Then, as in the classical way [12], we can show the error estimations by splitting spatial and temporal errors.

Before providing the stability bound, we want to introduce the following lemma in [24]:

Lemma 4.1. *Suppose $\boldsymbol{v}\in\boldsymbol{C}^1\left(0,T;\boldsymbol{\mathcal{D}}_k(\mathcal{E}_h)\right)$, γ_0 is large enough and $\gamma_1(d-1)\geq 1$. It holds that*

$$\begin{aligned}\int_0^T a\left({}_0I_t^{1-\alpha}\dot{\boldsymbol{v}}(t),\boldsymbol{v}(t)\right)dt\geq&\frac{1}{\Gamma(1-\alpha)}\int_0^T\xi_\alpha(t)\left\|\boldsymbol{v}(t)\right\|_V^2dt-\frac{1}{\Gamma(1-\alpha)}\int_0^T t^{-\alpha}a\left(\boldsymbol{v}(0),\boldsymbol{v}(t)\right)dt\\ \geq&\frac{T^{-\alpha}}{2^{-\alpha}\Gamma(1-\alpha)}\int_0^T\left\|\boldsymbol{v}(t)\right\|_V^2dt-\frac{1}{\Gamma(1-\alpha)}\int_0^T t^{-\alpha}a\left(\boldsymbol{v}(0),\boldsymbol{v}(t)\right)dt,\end{aligned}$$

where $\xi_\alpha(t)=((T-t)^{-\alpha}+t^{-\alpha})/2$.

Theorem 4.1. *Let $\boldsymbol{u}_h$ be the solution of* (3.7)-(3.8)*. Suppose $\boldsymbol{u}_h \in \boldsymbol{\mathcal{D}}_k(\mathcal{E}_h)$, γ_0 is large enough and $\gamma_1(d-1) \geq 1$. There exists a positive constant C such that*

$$\|\boldsymbol{u}_h\|^2_{L_2(0,T;V)} \leq C\bigg(T^\alpha \|\boldsymbol{f}\|^2_{L_2(0,T;L_2(\Omega))} + h^{-1}T^\alpha \|\boldsymbol{g}_N\|^2_{L_2(0,T;L_2(\Gamma_N))} + T^{1-\alpha}\|\boldsymbol{u}_0\|^2_{H^2(\Omega)}\bigg).$$

The constant C is independent of the solution, h and T.

Proof. Testing (3.7) with $\boldsymbol{v} = \boldsymbol{u}_h$ and using Lemma 4.1 leads us to obtain

$$\int_0^T \big\|\boldsymbol{u}_h(t)\big\|^2_V dt + \frac{1}{\Gamma(1-\alpha)}\int_0^T \xi_\alpha(t)\big\|\boldsymbol{u}_h(t)\big\|^2_V dt \leq \int_0^T F(\boldsymbol{u}_h(t))dt + \frac{1}{\Gamma(1-\alpha)}\int_0^T t^{-\alpha} a\left(\boldsymbol{u}_h(0), \boldsymbol{u}_h(t)\right) dt. \tag{4.1}$$

We shall show the bounds of the right hand side of (4.1). By Cauchy-Schwarz inequality, inverse polynomial trace inequality (2.1) and Poincaré's inequality (2.2), expanding the integration of the linear form yields

$$\int_0^T F(\boldsymbol{u}_h(t))dt \leq C\bigg(\int_0^T \big\|\boldsymbol{f}(t)\big\|_{L_2(\Omega)}\big\|\boldsymbol{u}_h(t)\big\|_V dt + h^{-1/2}\int_0^T \big\|\boldsymbol{g}_N(t)\big\|_{L_2(\Gamma_N)}\big\|\boldsymbol{u}_h(t)\big\|_V dt\bigg),$$

where C is a positive constant from the trace inequality and the Poincaré inequality. Using Young's inequalities, we can deduce that

$$\int_0^T F(\boldsymbol{u}_h(t))dt \leq \int_0^T \left(\frac{\epsilon_a}{2} + \frac{\epsilon_b}{2}\right)\big\|\boldsymbol{u}_h(t)\big\|^2_V dt + C\left(\int_0^T \frac{1}{2\epsilon_a}\big\|\boldsymbol{f}(t)\big\|^2_{L_2(\Omega)} dt + h^{-1}\int_0^T \frac{1}{2\epsilon_b}\big\|\boldsymbol{g}_N(t)\big\|^2_{L_2(\Gamma_N)} dt\right), \tag{4.2}$$

for any positive ϵ_a and ϵ_b.

Similarly, applying Cauchy-Schwarz inequality, Young's inequality and the continuity of the DG bilinear form yields

$$\frac{1}{\Gamma(1-\alpha)}\int_0^T t^{-\alpha} a\left(\boldsymbol{u}_h(0), \boldsymbol{u}_h(t)\right) dt \leq \frac{1}{\Gamma(1-\alpha)}\int_0^T \frac{\epsilon_c}{2}\big\|\boldsymbol{u}_h(t)\big\|^2_V dt + \frac{K^2}{\Gamma(1-\alpha)}\int_0^T \frac{1}{2\epsilon_c} t^{-2\alpha}\big\|\boldsymbol{u}_h(0)\big\|^2_V dt, \tag{4.3}$$

for positive ϵ_c. Since (3.8) implies that

$$\big\|\boldsymbol{u}_h(0)\big\|_V \leq C\big\|\boldsymbol{u}_0\big\|_V, \tag{4.4}$$

we can write (4.3) as

$$\frac{1}{\Gamma(1-\alpha)}\int_0^T t^{-\alpha} a\left(\boldsymbol{u}_h(0), \boldsymbol{u}_h(t)\right) dt \leq \frac{1}{\Gamma(1-\alpha)}\int_0^T \frac{\epsilon_c}{2}\big\|\boldsymbol{u}_h(t)\big\|^2_V dt + \frac{C}{\Gamma(1-\alpha)}\int_0^T \frac{1}{2\epsilon_c} t^{-2\alpha}\|\boldsymbol{u}_0\|^2_{H^2(\Omega)} dt. \tag{4.5}$$

Here, the positive constant C is independent of the solution, h and time and we refer to [38] for more details of (4.4).

Tidying up the results of (4.2) and (4.5), the setting of ϵ_a, ϵ_b and ϵ_c by

$$\epsilon_a = \epsilon_b = \frac{\xi_\alpha(t)}{4\Gamma(1-\alpha)}, \qquad \text{and} \qquad \epsilon_c = \xi_\alpha(t),$$

gives

$$\begin{aligned}\int_0^T \big\|\boldsymbol{u}_h(t)\big\|^2_V dt \leq C\bigg(&\int_0^T (\xi_\alpha(t))^{-1}\big\|\boldsymbol{f}(t)\big\|^2_{L_2(\Omega)} dt + h^{-1}\int_0^T (\xi_\alpha(t))^{-1}\big\|\boldsymbol{g}_N(t)\big\|^2_{L_2(\Gamma_N)} dt \\ &+ \int_0^T (\xi_\alpha(t))^{-1} t^{-2\alpha} dt\,\|\boldsymbol{u}_0\|^2_{H^2(\Omega)}\bigg),\end{aligned}$$

for some positive C. We note that for any integrable $\phi(t)$,

$$\int_0^T (\xi_\alpha(t))^{-1}\phi(t)dt = \int_0^T \frac{2\phi(t)}{(T-t)^{-\alpha} + t^{-\alpha}} dt \leq \int_0^T \frac{2\phi(t)}{t^{-\alpha}} dt \leq 2T^\alpha \int_0^T \phi(t)dt,$$

and

$$\int_0^T (\xi_\alpha(t))^{-1} t^{-2\alpha} dt = \int_0^T \frac{2t^{-2\alpha}}{(T-t)^{-\alpha} + t^{-\alpha}} dt \leq \int_0^T \frac{2t^{-2\alpha}}{t^{-\alpha}} dt = \frac{2T^{1-\alpha}}{1-\alpha}.$$

Consequently, we have

$$\int_0^T \big\|\boldsymbol{u}_h(t)\big\|^2_V dt \leq C\bigg(T^\alpha \int_0^T \big\|\boldsymbol{f}(t)\big\|^2_{L_2(\Omega)} dt + h^{-1}T^\alpha \int_0^T \big\|\boldsymbol{g}_N(t)\big\|^2_{L_2(\Gamma_N)} dt + T^{1-\alpha}\|\boldsymbol{u}_0\|^2_{H^2(\Omega)}\bigg).$$

□

The stability bound in Theorem 4.1 reveals the presence of h^{-1} term. This term arises from the inverse polynomial trace inequality but does not significantly affect practical applications. It implies only that the Neumann boundary condition is weakly imposed; see also [26, 38] for further discussion.

In this stability analysis, we do not employ the positive definiteness (2.4). On the other hand, as described in [12], we can show $L_\infty(V)$ stability using the positive definiteness. Unlike typical momentum equations, our quasi-static model problems do not involve acceleration. Consequently, to manage the spatial stability of velocity, we need to introduce additional regularity in the data terms.

For the convention of notation, let us denote a Laplace convolution by $*$, and define $\beta_{1-\alpha}(t) = t^{-\alpha}/\Gamma(1-\alpha)$ and $\mathcal{A} = -\nabla\cdot\underline{\boldsymbol{D}}\underline{\boldsymbol{\varepsilon}}$. With these definitions, we can rewrite (3.3) as

$$\boldsymbol{f}(t) = \varphi_0\mathcal{A}\boldsymbol{u}(t) + \varphi_\alpha\beta_{1-\alpha} * \mathcal{A}\dot{\boldsymbol{u}}(t). \tag{4.6}$$

Differentiating (4.6) gives

$$\dot{\boldsymbol{f}}(t) = \varphi_0\mathcal{A}\dot{\boldsymbol{u}}(t) + \varphi_\alpha\beta_{1-\alpha}(t)\mathcal{A}\boldsymbol{w}_0 + \varphi_\alpha\beta_{1-\alpha} * \mathcal{A}\ddot{\boldsymbol{u}}(t). \tag{4.7}$$

If the quasi-static state allows for negligible acceleration, we have

$$\dot{\boldsymbol{f}}(t) = \varphi_0\mathcal{A}\dot{\boldsymbol{u}}(t) + \varphi_\alpha\beta_{1-\alpha}(t)\mathcal{A}\boldsymbol{w}_0, \tag{4.8}$$

and $\dot{\boldsymbol{f}}$ is clearly L_1 integrable in time for L_1 integrable $\mathcal{A}\dot{\boldsymbol{u}}$. However, since $\beta_{1-\alpha}$ is only L_1 integrable, the necessary condition of L_2 integrability of $\boldsymbol{f}$ follows

$$\mathcal{A}\dot{\boldsymbol{u}} \in \boldsymbol{L}_2(0,T) \qquad \text{and} \qquad \boldsymbol{w}_0 \in \ker(\mathcal{A}), \tag{4.9}$$

where $\ker(\mathcal{A})$ is the kernel of the differential operator $\mathcal{A}$.

Theorem 4.2. *Let $\boldsymbol{u}_h$ be a solution of the semi-discrete problem* (3.7)-(3.8)*. Suppose $\boldsymbol{u}_h \in \boldsymbol{L}_\infty(0,T;\boldsymbol{H}^s(\mathcal{E}_h))$ and $\boldsymbol{g}_N \in \boldsymbol{C}^1(0,T;\boldsymbol{L}_2(\Gamma_N))$. Furthermore, we assume that* (4.9) *holds or $\boldsymbol{f} \in \boldsymbol{C}^1(0,T;\boldsymbol{L}_2(\Gamma_N))$. If γ_0 is large enough and $\gamma_1(d-1) \geq 1$, there exists a positive constant C such that*

$$\begin{aligned}\|\boldsymbol{u}_h\|^2_{L_\infty(0,T;V)} \leq C\Bigg(&\|\boldsymbol{u}_0\|^2_{H^2(\Omega)} + \|\boldsymbol{f}\|^2_{L_\infty(0,T;L_2(\Omega))} + T\left\|\dot{\boldsymbol{f}}\right\|^2_{L_2(0,T;L_2(\Omega))} + h^{-1}\|\boldsymbol{g}_N\|^2_{L_\infty(0,T;L_2(\Gamma_N))} \\ &+ h^{-1}T\|\dot{\boldsymbol{g}}_N\|^2_{L_2(0,T;L_2(\Gamma_N))}\Bigg).\end{aligned}$$

The constant C is independent of the semi-discrete solution, T and h.

Proof. The proof follows similar arguments to those in [12, Theorem 1]. Instead of testing with the displacement, we use the velocity. This allows us to immediately apply the positive definiteness property of fractional integration (2.4). However, due to the absence of acceleration in our model problem, we need further estimations of velocity terms in the linear form with integration by parts.

Let $\boldsymbol{v} = \dot{\boldsymbol{u}}_h(t)$ in (3.7). For $0 < \tau \leq T$, integration over time gives

$$\begin{aligned}\frac{\varphi_0}{2}\left\|\boldsymbol{u}_h(\tau)\right\|^2_V + \varphi_\alpha\int_0^\tau a\left({}_0I_t^{1-\alpha}\dot{\boldsymbol{u}}_h(t), \dot{\boldsymbol{u}}_h(t)\right)dt = &\int_0^\tau F(\dot{\boldsymbol{u}}_h(t)) + \frac{\varphi_0}{2}\left\|\boldsymbol{u}_h(0)\right\|^2_V \\ &+ \varphi_0\sum_{e\subset\Gamma_h\cup\Gamma_D}\int_e\{\underline{\boldsymbol{D}}\underline{\boldsymbol{\varepsilon}}(\boldsymbol{u}_h(\tau))\} : [\boldsymbol{u}_h(\tau)\otimes\boldsymbol{n}_e]\,de \\ &- \varphi_0\sum_{e\subset\Gamma_h\cup\Gamma_D}\int_e\{\underline{\boldsymbol{D}}\underline{\boldsymbol{\varepsilon}}(\boldsymbol{u}_h(0))\} : [\boldsymbol{u}_h(0)\otimes\boldsymbol{n}_e]\,de,\end{aligned} \tag{4.10}$$

by expanding the bilinear form. Since

$$\int_0^\tau a\left({}_0I_t^{1-\alpha}\dot{\boldsymbol{u}}_h(t), \dot{\boldsymbol{u}}_h(t)\right)dt \geq 0,$$

by (2.4), we have

$$\begin{aligned}\frac{\varphi_0}{2}\left\|\boldsymbol{u}_h(\tau)\right\|^2_V \leq \int_0^\tau F(\dot{\boldsymbol{u}}_h(t)) + \frac{\varphi_0}{2}\left\|\boldsymbol{u}_h(0)\right\|^2_V + \varphi_0\sum_{e\subset\Gamma_h\cup\Gamma_D}\int_e\{\underline{\boldsymbol{D}}\underline{\boldsymbol{\varepsilon}}(\boldsymbol{u}_h(\tau))\} : [\boldsymbol{u}_h(\tau)\otimes\boldsymbol{n}_e]\,de \\ - \varphi_0\sum_{e\subset\Gamma_h\cup\Gamma_D}\int_e\{\underline{\boldsymbol{D}}\underline{\boldsymbol{\varepsilon}}(\boldsymbol{u}_h(0))\} : [\boldsymbol{u}_h(0)\otimes\boldsymbol{n}_e]\,de.\end{aligned} \tag{4.11}$$

Also, (3.14) implies that

$$\sum_{e\subset\Gamma_h\cup\Gamma_D}\int_e(\{\underline{\boldsymbol{D}}\underline{\boldsymbol{\varepsilon}}(\boldsymbol{u}_h(\tau))\}:[\boldsymbol{u}_h(\tau)\otimes\boldsymbol{n}_e]-\{\underline{\boldsymbol{D}}\underline{\boldsymbol{\varepsilon}}(\boldsymbol{u}_h(0))\}:[\boldsymbol{u}_h(0)\otimes\boldsymbol{n}_e])\leq\frac{C}{\sqrt{\gamma_0}}\left(\|\boldsymbol{u}_h\|^2_{L_\infty(0,T;V)}+\|\boldsymbol{u}_0\|^2_{H^2(\Omega)}\right), \tag{4.12}$$

for some positive C. Hence, with (4.4), we can obtain

$$\frac{\varphi_0}{2}\|\boldsymbol{u}_h(\tau)\|^2_V\leq\int_0^\tau F(\dot{\boldsymbol{u}}_h(t))+\left(\frac{\varphi_0}{2}+\frac{C}{\sqrt{\gamma_0}}\right)\|\boldsymbol{u}_0\|^2_{H^2(\Omega)}+\frac{C}{\sqrt{\gamma_0}}\|\boldsymbol{u}_h\|^2_{L_\infty(0,T;V)}. \tag{4.13}$$

Next, we shall show the bound of the linear form term. From the definition of the linear form, integration by parts leads to

$$\begin{aligned}\int_0^\tau F(\dot{\boldsymbol{u}}_h(t))dt&=\int_0^\tau(\boldsymbol{f}(t),\dot{\boldsymbol{u}}_h(t))\,dt+\int_0^\tau(\boldsymbol{g}_N(t),\dot{\boldsymbol{u}}_h(t))_{L_2(\Gamma_N)}\,dt\\&=(\boldsymbol{f}(\tau),\boldsymbol{u}_h(\tau))-(\boldsymbol{f}(0),\boldsymbol{u}_h(0))-\int_0^\tau\left(\dot{\boldsymbol{f}}(t),\boldsymbol{u}_h(t)\right)dt\\&\quad+(\boldsymbol{g}_N(\tau),\boldsymbol{u}_h(\tau))_{L_2(\Gamma_N)}-(\boldsymbol{g}_N(0),\boldsymbol{u}_h(0))_{L_2(\Gamma_N)}-\int_0^\tau(\dot{\boldsymbol{g}}_N(t),\boldsymbol{u}_h(t))_{L_2(\Gamma_N)}\,dt.\end{aligned} \tag{4.14}$$

As in the proof of Theorem 4.1, using Cauchy-Schwarz inequality, Poincaré inequality and inverse polynomial trace inequality, we derive

$$\begin{aligned}\int_0^\tau F(\dot{\boldsymbol{u}}_h(t))dt\leq C\Bigg(&\|\boldsymbol{f}(\tau)\|_{L_2(\Omega)}\|\boldsymbol{u}_h(\tau)\|_V+\|\boldsymbol{f}(0)\|_{L_2(\Omega)}\|\boldsymbol{u}_h(0)\|_V\\&+\int_0^\tau\|\dot{\boldsymbol{f}}(t)\|_{L_2(\Omega)}\|\boldsymbol{u}_h(t)\|_V dt+h^{-1/2}\|\boldsymbol{g}_N(\tau)\|_{L_2(\Gamma_N)}\|\boldsymbol{u}_h(\tau)\|_V\\&+h^{-1/2}\|\boldsymbol{g}_N(0)\|_{L_2(\Gamma_N)}\|\boldsymbol{u}_h(0)\|_V+h^{-1/2}\int_0^\tau\|\dot{\boldsymbol{g}}_N(t)\|_{L_2(\Gamma_N)}\|\boldsymbol{u}_h(t)\|_V dt\Bigg).\end{aligned} \tag{4.15}$$

Taking into account L_∞ arguments in time for $\boldsymbol{u}_h$, employing Young's inequalities and (4.4) yields

$$\begin{aligned}\int_0^\tau F(\dot{\boldsymbol{u}}_h(t))dt\leq C\Bigg(&\frac{\epsilon_a+\epsilon_b+\epsilon_c+\epsilon_d}{2}\|\boldsymbol{u}_h\|_{L_\infty(0,T;H^s(\mathcal{E}_h))}+\frac{1}{2\epsilon_a}\|\boldsymbol{f}\|^2_{L_\infty(0,T;L_2(\Omega))}\\&+\frac{1}{2}\|\boldsymbol{f}\|^2_{L_\infty(0,T;L_2(\Omega))}+\frac{T}{2\epsilon_b}\left\|\dot{\boldsymbol{f}}\right\|^2_{L_2(0,T;L_2(\Omega))}\\&+\|\boldsymbol{u}_0\|^2_{H^2(\Omega)}+\frac{h^{-1}}{2\epsilon_c}\|\boldsymbol{g}_N\|^2_{L_\infty(0,T;L_2(\Gamma_N))}\\&+\frac{h^{-1}}{2}\|\boldsymbol{g}_N\|^2_{L_\infty(0,T;L_2(\Gamma_N))}+\frac{h^{-1}T}{2\epsilon_d}\|\dot{\boldsymbol{g}}_N\|^2_{L_2(0,T;L_2(\Gamma_N))}\Bigg),\end{aligned} \tag{4.16}$$

for any positive ϵ_a, ϵ_b, ϵ_c and ϵ_d. After noting that τ is arbitrary, combining (4.13) with (4.16) gives

$$\begin{aligned}\left(\frac{\varphi_0}{4}-\frac{C}{\sqrt{\gamma_0}}\right)\|\boldsymbol{u}_h\|^2_{L_\infty(0,T;V)}\leq C\Bigg(&\|\boldsymbol{u}_0\|^2_{H^2(\Omega)}+\|\boldsymbol{f}\|^2_{L_\infty(0,T;L_2(\Omega))}+T\left\|\dot{\boldsymbol{f}}\right\|^2_{L_2(0,T;L_2(\Omega))}+h^{-1}\|\boldsymbol{g}_N\|^2_{L_\infty(0,T;L_2(\Gamma_N))}\\&+h^{-1}T\|\dot{\boldsymbol{g}}_N\|^2_{L_2(0,T;L_2(\Gamma_N))}\Bigg),\end{aligned} \tag{4.17}$$

by setting $\epsilon_a=\epsilon_b=\epsilon_c=\epsilon_d=\varphi_0/(8C)$. Therefore, taking large γ_0 satisfying $\varphi_0/4-C/\sqrt{\gamma_0}>0$ completes the proof. □

The L_∞ stability analysis in Theorem 4.2 is similar to the stability bound in [12]. However, in our proof, since our primal model problem does not contain the inertial force, we rather introduce integration by parts to deal with discrete velocity. As a result, our stability bound requires more regularity in the body force and the traction force. In this manner, we can provide a stability bound of the fully discrete case. For example, as in the semi-discrete problem, using trace inequalities, Poincaré inequalities, Young's inequalities, etc., allows us to prove the L_∞ stability bound. Instead of introducing the positive definiteness property in fractional integration, we employ mathematical induction. We refer to the work of Jang and Shaw [12] for all technical details.

Theorem 4.3. *If $\gamma_1(d-1) \geq 1$ and γ_0 is sufficiently large, there exists a unique discrete solution to* (3.18)-(3.19) *that satisfies*

$$\max_{0\leq n\leq N}\left\|\boldsymbol{U}_h^n\right\|_V^2+\Delta t^{2-\alpha}\sum_{n=0}^{N-1}\left\|\boldsymbol{W}_h^{n+1}+\boldsymbol{W}_h^n\right\|_V^2\leq C\Bigg(\|\boldsymbol{w}_0\|_{H^2(\Omega)}^2+\|\boldsymbol{u}_0\|_{H^2(\Omega)}^2 + \max_{0\leq n\leq N}\left\|\boldsymbol{f}(t_n)\right\|_{L_2(\Omega)}^2+T\left\|\dot{\boldsymbol{f}}\right\|_{L_2(0,T;L_2(\Omega))}^2 + h^{-1}\max_{0\leq n\leq N}\left\|\boldsymbol{g}_N(t_n)\right\|_{L_2(\Gamma_N)}^2+h^{-1}T\left\|\dot{\boldsymbol{g}}_N\right\|_{L_2(0,T;L_2(\Gamma_N))}^2\Bigg).$$

where C is independent of the solution, Δt and h.

Proof. Our proof follows the approach outlined in [12, Theorem 2], where all arguments are thoroughly explained and applicable to our context. Without providing all technical details, we show the bounds for the linear form.

Let $m < N$ be an arbitrary positive integer. With using

$$\boldsymbol{v}=2\Delta t(\boldsymbol{W}_h^{n+1}+\boldsymbol{W}_h^n)=4(\boldsymbol{U}_h^{n+1}-\boldsymbol{U}_h^n)$$

by (3.17) for $0\leq n\leq m-1$, the substitution of $\boldsymbol{v}$ into (3.18) and the summation from $n=0$ to $n=m-1$ lead us to get

$$\begin{aligned}&2\varphi_0 a\left(\boldsymbol{U}_h^m,\boldsymbol{U}_h^m\right)+\varphi_\alpha\Delta t\sum_{n=0}^{m-1}a\left(\boldsymbol{Q}_{n+1}(\boldsymbol{W}_h)+\boldsymbol{Q}_n(\boldsymbol{W}_h),\boldsymbol{W}_h^{n+1}+\boldsymbol{W}_h^n\right)\\ =&2\varphi_0 a\left(\boldsymbol{U}_h^0,\boldsymbol{U}_h^0\right)+2\sum_{n=0}^{m-1}\left(\boldsymbol{f}(t_{n+1})+\boldsymbol{f}(t_n),\boldsymbol{U}_h^{n+1}-\boldsymbol{U}_h^n\right)+2\sum_{n=0}^{m-1}\left(\boldsymbol{g}_N(t_{n+1})+\boldsymbol{g}_N(t_n),\boldsymbol{U}_h^{n+1}-\boldsymbol{U}_h^n\right)_{L_2(\Gamma_N)},\end{aligned}$$

and expanding the discrete fractional integration and the coercivity yield

$$\begin{aligned}&2\kappa\varphi_0\left\|\boldsymbol{U}_h^m\right\|_V^2+\frac{\kappa\varphi_\alpha\Delta t^{2-\alpha}}{\Gamma(3-\alpha)}\sum_{n=0}^{m-1}\left\|\boldsymbol{W}_h^{n+1}+\boldsymbol{W}_h^n\right\|_V^2\\ \leq&2\varphi_0 a\left(\boldsymbol{U}_h^0,\boldsymbol{U}_h^0\right)+2\sum_{n=0}^{m-1}\left(\boldsymbol{f}(t_{n+1})+\boldsymbol{f}(t_n),\boldsymbol{U}_h^{n+1}-\boldsymbol{U}_h^n\right)+2\sum_{n=0}^{m-1}\left(\boldsymbol{g}_N(t_{n+1})+\boldsymbol{g}_N(t_n),\boldsymbol{U}_h^{n+1}-\boldsymbol{U}_h^n\right)_{L_2(\Gamma_N)}\\ &-\frac{\varphi_\alpha\Delta t^{2-\alpha}}{\Gamma(3-\alpha)}\sum_{n=0}^{m-1}a\left(\sum_{i=0}^{n}B_{n+1,i}\boldsymbol{W}_h^i+\sum_{i=0}^{n-1}B_{n,i}\boldsymbol{W}_h^i,\boldsymbol{W}_h^{n+1}+\boldsymbol{W}_h^n\right),\end{aligned}\tag{4.18}$$

We consider the bound of the second term in the right hand side of (4.18). By summation by parts, we have

$$2\sum_{n=0}^{m-1}\left(\boldsymbol{f}(t_{n+1})+\boldsymbol{f}(t_n),\boldsymbol{U}_h^{n+1}-\boldsymbol{U}_h^n\right)=2\left(\boldsymbol{f}(t_m),\boldsymbol{U}_h^m\right)-2\left(\boldsymbol{f}(0),\boldsymbol{U}_h^0\right)-2\sum_{n=0}^{m-1}\left(\boldsymbol{f}(t_{n+1})-\boldsymbol{f}(t_n),\boldsymbol{U}_h^{n+1}+\boldsymbol{U}_h^n\right).\tag{4.19}$$

The fundamental theorem of calculus immediately gives

$$\begin{aligned}2\sum_{n=0}^{m-1}\left(\boldsymbol{f}(t_{n+1})+\boldsymbol{f}(t_n),\boldsymbol{U}_h^{n+1}-\boldsymbol{U}_h^n\right)=&2\left(\boldsymbol{f}(t_m),\boldsymbol{U}_h^m\right)-2\left(\boldsymbol{f}(0),\boldsymbol{U}_h^0\right)-2\sum_{n=0}^{m-1}\left(\int_{t_n}^{t_{n+1}}\dot{\boldsymbol{f}}(t)dt,\boldsymbol{U}_h^{n+1}+\boldsymbol{U}_h^n\right)\\ =&2\left(\boldsymbol{f}(t_m),\boldsymbol{U}_h^m\right)-2\left(\boldsymbol{f}(0),\boldsymbol{U}_h^0\right)-2\sum_{n=0}^{m-1}\int_{t_n}^{t_{n+1}}\left(\dot{\boldsymbol{f}}(t),\boldsymbol{U}_h^{n+1}+\boldsymbol{U}_h^n\right)dt,\end{aligned}\tag{4.20}$$

then combining Cauchy-Schwarz inequality, Poincaré inequality, Young's inequality and (3.19) as in a previous manner implies

$$\begin{aligned}&2\sum_{n=0}^{m-1}\left(\boldsymbol{f}(t_{n+1})+\boldsymbol{f}(t_n),\boldsymbol{U}_h^{n+1}-\boldsymbol{U}_h^n\right)\\ \leq&C\Bigg(\frac{1}{\epsilon_a}\max_{0\leq n\leq N}\left\|\boldsymbol{f}(t_n)\right\|_{L_2(\Omega)}^2+\epsilon_a\left\|\boldsymbol{U}_h^m\right\|_V^2+\max_{0\leq n\leq N}\left\|\boldsymbol{f}(t_n)\right\|_{L_2(\Omega)}^2+\|\boldsymbol{u}_0\|_{H^2(\Omega)}\end{aligned}$$

$$
\begin{aligned}
&+\sum_{n=0}^{m-1}\int_{t_n}^{t_{n+1}}\frac{1}{\epsilon_b}\big\|\dot{\boldsymbol{f}}(t)\big\|_{L_2(\Omega)}^2+\epsilon_b\big\|\boldsymbol{U}_h^{n+1}+\boldsymbol{U}_h^n\big\|_V^2dt\Big)\\
\leq& C\Big(\frac{1+\epsilon_a}{\epsilon_a}\max_{0\leq n\leq N}\big\|\boldsymbol{f}(t_n)\big\|_{L_2(\Omega)}^2+\big(\epsilon_a+2\epsilon_b\sum_{n=0}^{N-1}\int_{t_n}^{t_{n+1}}dt\big)\max_{0\leq n\leq N}\big\|\boldsymbol{U}_h^n\big\|_V^2+\|\boldsymbol{u}_0\|_{H^2(\Omega)}\\
&+\sum_{n=0}^{N-1}\int_{t_n}^{t_{n+1}}\frac{1}{\epsilon_b}\big\|\dot{\boldsymbol{f}}(t)\big\|_{L_2(\Omega)}^2dt\Big)\\
=& C\Big(\frac{1+\epsilon_a}{\epsilon_a}\max_{0\leq n\leq N}\big\|\boldsymbol{f}(t_n)\big\|_{L_2(\Omega)}^2+(\epsilon_a+2\epsilon_bT)\max_{0\leq n\leq N}\big\|\boldsymbol{U}_h^n\big\|_V^2+\|\boldsymbol{u}_0\|_{H^2(\Omega)}+\frac{1}{\epsilon_b}\Big\|\dot{\boldsymbol{f}}\Big\|_{L_2(0,T;L_2(\Omega))}^2\Big),
\end{aligned}
\tag{4.21}
$$

where C is the positive constant depending on Poincaré inequality. In the same way in (4.21), we can obtain the bound of the third term of the right hand side of (4.18).

To end the proof, the bound of the last term in (4.18) is required. Using mathematical induction, we can observe the cancellation of the last term by the initial condition of velocity and the left hand side term,

$$
\frac{\kappa\varphi_\alpha\Delta t^{2-\alpha}}{\Gamma(3-\alpha)}\sum_{n=0}^{m-1}\big\|\boldsymbol{W}_h^{n+1}+\boldsymbol{W}_h^n\big\|_V^2.
$$

We refer to [12] for the induction process in our context. Consequently, we complete the proof by taking a large enough γ_0 and defining appropriate coefficients of Young's inequality. □

Our stability analysis implies the existence and uniqueness of the solution for the discrete quasi-static viscoelastic problem of the power-law type. The stability bound has been shown in similar ways with the dynamic viscoelasticity cases but it requires higher regularity of the data terms. More specifically, due to the absence of the inertial force in our primal model problem, we must introduce integration by parts or summation by parts to replace discrete velocity with discrete displacement. As a consequence, we need more smoothness of the body force and traction.

Next, we consider the *a priori* error analysis of the fully discrete problem. For the *a priori* error estimate, we first introduce an elliptic projector. The DG elliptic projector [26, 39, 20, 40], $\boldsymbol{R}$, is defined for $\boldsymbol{u}\in\boldsymbol{H}^s(\mathcal{E}_h)$ and $s>3/2$ by,

$$
\boldsymbol{R}:\boldsymbol{H}^s(\mathcal{E}_h)\mapsto\boldsymbol{\mathcal{D}}_k(\mathcal{E}_h)\ \text{ such that }\ a\left(\boldsymbol{u},\boldsymbol{v}\right)=a\left(\boldsymbol{Ru},\boldsymbol{v}\right),\ \forall\boldsymbol{v}\in\boldsymbol{\mathcal{D}}_k(\mathcal{E}_h).
$$

Note that we have the Galerkin orthogonality such that $a\left(\boldsymbol{u}-\boldsymbol{Ru},\boldsymbol{v}\right)=0$ for any $\boldsymbol{v}\in\boldsymbol{\mathcal{D}}_k(\mathcal{E}_h)$, and the following elliptic-error estimates,

$$
\big\|\boldsymbol{u}-\boldsymbol{Ru}\big\|_V\leq Ch^{\min(k+1,s)-1}|||\boldsymbol{u}|||_{H^s(\mathcal{E}_h)},\qquad\text{and}\qquad\big\|\boldsymbol{u}-\boldsymbol{Ru}\big\|_{L_2(\Omega)}\leq Ch^{\min(k+1,s)}|||\boldsymbol{u}|||_{H^s(\mathcal{E}_h)},
\tag{4.22}
$$

for $\boldsymbol{u}\in\boldsymbol{H}^s(\mathcal{E}_h)$ with $s>3/2$ and for sufficiently large penalty parameters $\gamma_0>0$ and $\gamma_1\geq(d-1)^{-1}$. Here, the positive constant C is independent of $\boldsymbol{u}$ but dependent on the domain, its boundary, and the polynomial degree k.

Theorem 4.4. *Assume that*

$$
\boldsymbol{u}\in\boldsymbol{C}^2\left(0,T;\boldsymbol{C}^2(\Omega)\cap\boldsymbol{H}^s(\mathcal{E}_h)\right)\cap\boldsymbol{W}_\infty^3(0,T;\boldsymbol{H}^s(\mathcal{E}_h)),
$$

$\boldsymbol{f}$, $\boldsymbol{g}_N$ and initial conditions are sufficiently smooth to hold Theorem 4.3, and $(\boldsymbol{U}_h^n)_{n=0}^N$ and $(\boldsymbol{W}_h^n)_{n=0}^N$ are the fully discrete solution. Then we observe optimal orders of L_2 error estimates as well as energy error estimates with respect to h, and second-order accuracy in time by Crank-Nicolson type approximations. Thus, we obtain

$$
\max_{0\leq n\leq N}\big\|\boldsymbol{u}(t_n)-\boldsymbol{U}_h^n\big\|_{L_2(\Omega)}\leq CT^{2-\alpha}\big(h^r+\Delta t^2\big),\qquad\textit{and}\qquad\max_{0\leq n\leq N}\big\|\boldsymbol{u}(t_n)-\boldsymbol{U}_h^n\big\|_V\leq CT^{2-\alpha}\big(h^{r-1}+\Delta t^2\big),
$$

where $r=\min(k+1,s)$ and C is a positive constant independent of h and Δt.

Proof. Using the DG elliptic operator, we can decompose the spatial error by

$$
\boldsymbol{u}(t_n)-\boldsymbol{U}_h^n=\left(\boldsymbol{u}(t_n)-\boldsymbol{Ru}(t_n)\right)+\left(\boldsymbol{Ru}(t_n)-\boldsymbol{U}_h^n\right).
$$

The proof follows the same approach as that of the dynamic problem. Please refer to the work of Jang and Shaw[12] for details. We remark that the quasi-static state can impose negligible acceleration hence the Crank-Nicolson scheme provides the optimal second order accuracy without further regularity of solution such as H^4 regularity in time as is necessary in the dynamic problem. □

Remark 3. *Compared to the dynamic model problem[11, 12], our fully discrete formulation does not require any jump penalty of velocity or acceleration. Indeed, we can add it to the fully discrete form but it would not affect the stability and error estimates but only enables us to control the spatial discontinuity on numerical velocity.*

5 A posteriori analysis

In this section, we present *a posteriori* error estimation of the semi-discrete problem. Following the approach used in the linear elastic problem [20, 21], we construct an error estimator $\eta_{\text{err}}(t)$ and a data oscillation term $osc(t)$. Our goal is to demonstrate that

$$\left\|\boldsymbol{u}(t)-\boldsymbol{u}_h(t)\right\|_V \leq C\left(\eta_{\text{err}}(t)+osc(t)\right),$$

for the exact solution $\boldsymbol{u}$ and the semi-discrete solution $\boldsymbol{u}_h$, where C is independent of solutions. For the sake of simplicity, we use the notation '$\lesssim$', for instance, $A \lesssim B$ indicates that $A \leq CB$, where C is a positive constant independent of A and B.

To define the error estimator and the data oscillation term, we first denote the discrete version of data terms. For example, $\boldsymbol{u}_{0,h}$, $\boldsymbol{f}_h$ and $\boldsymbol{g}_{N,h}$ are the L_2 projections of $\boldsymbol{u}_0$, $\boldsymbol{f}$ and $\boldsymbol{g}_N$ onto the finite element space, respectively. Using the discrete data terms, we can define the *a posteriori* error estimator by

$$\eta_{\text{err}}^2(t)=\sum_{E\in\mathcal{E}_h}\left(\eta_{1,E}^2(t)+\eta_{2,E}^2(t)+\eta_{3,E}^2(t)\right), \tag{5.1}$$

where

$$\eta_{1,E}^2(t)=h_E^2\left\|\boldsymbol{f}_h(t)+\nabla\cdot\underline{\boldsymbol{\sigma}}(\boldsymbol{u}_h(t))\right\|_{L_2(E)}^2, \tag{5.2}$$

$$\eta_{2,E}^2(t)=\sum_{e\subset\partial E\cap(\Gamma_h\cup\Gamma_D)}|e|^{-1}\left(\left\|[\![\boldsymbol{u}_h(t)]\!]\right\|_{L_2(e)}^2+\left\|[\![{}_0I_t^{1-\alpha}\dot{\boldsymbol{u}}_h(t)]\!]\right\|_{L_2(e)}^2\right), \tag{5.3}$$

$$\eta_{3,E}^2(t)=\sum_{e\subset\partial E\cap\Gamma_h}|e|\left\|[\![\underline{\boldsymbol{\sigma}}(\boldsymbol{u}_h(t))]\!]\right\|_{L_2(e)}^2+\sum_{e\subset\partial E\cap\Gamma_N}|e|\left\|\underline{\boldsymbol{\sigma}}(\boldsymbol{u}_h(t))\cdot\boldsymbol{n}_e-\boldsymbol{g}_{N,h}(t)\right\|_{L_2(e)}^2. \tag{5.4}$$

Also, we can introduce the oscillation term:

$$osc^2(t)=\|\boldsymbol{u}_0-\boldsymbol{u}_{0,h}\|_{H^1(\Omega)}^2+osc_1^2(t)+\sum_{E\in\mathcal{E}_h}\left(osc_{2,E}^2(t)+osc_{3,E}^2(t)\right), \tag{5.5}$$

where

$$osc_1^2(t)=\left\|\boldsymbol{g}_N(t)-\boldsymbol{g}_{N,h}(t)\right\|_{L_2(\Gamma_N)}^2+\|\dot{\boldsymbol{g}}_N-\dot{\boldsymbol{g}}_{N,h}\|_{L_2(0,t;L_2(\Gamma_N))}, \tag{5.6}$$

$$osc_{2,E}^2(t)=h_E^2\left\|\boldsymbol{f}(t)-\boldsymbol{f}_h(t)\right\|_{L_2(E)}^2, \tag{5.7}$$

$$osc_{3,E}^2(t)=\sum_{e\subset\partial E\cap\Gamma_N}|e|\left\|\boldsymbol{g}_N(t)-\boldsymbol{g}_{N,h}(t)\right\|_{L_2(e)}^2, \tag{5.8}$$

For the analysis of the *a posteriori* error estimation, we follow a similar process to that used in the linear elasticity problem[21]. Although our model problem contains a weak singularity in the constitutive equation, it remains a linear problem. Therefore, we can show the error estimation by introducing an auxiliary continuous problem and splitting the error using a conforming and nonconforming decomposition. We refer to [20, 40, 21, 41] and the references therein for the technical details of *a posteriori* analysis.

Next, we give a continuous problem to manage the data oscillation. Suppose $\boldsymbol{U}(t)$ is the solution to

$$-\nabla\cdot\underline{\boldsymbol{\sigma}}(\boldsymbol{U}(t))=\boldsymbol{f}(t) \qquad \text{in } \Omega\times(0,T], \tag{5.9}$$

$$\boldsymbol{U}(t)=\boldsymbol{0} \qquad \text{on } \Gamma_D, \tag{5.10}$$

$$\underline{\boldsymbol{\sigma}}(\boldsymbol{U}(t))\cdot\boldsymbol{n}=\boldsymbol{g}_{N,h}(t) \qquad \text{on } \Gamma_N, \tag{5.11}$$

$$\boldsymbol{U}(0)=\boldsymbol{u}_{0,h} \qquad \text{in } \Omega, \tag{5.12}$$

and $\boldsymbol{U}(t)\in\boldsymbol{H}^1(\Omega)$. We define the continuous analogue of energy norm by

$$\left\|\boldsymbol{v}\right\|_D^2:=\int_\Omega\underline{\boldsymbol{D}}\underline{\boldsymbol{\varepsilon}}(\boldsymbol{v}):\underline{\boldsymbol{\varepsilon}}(\boldsymbol{v})d\Omega, \tag{5.13}$$

for $\boldsymbol{v}\in\boldsymbol{H}^1(\Omega)$. If $\boldsymbol{v}$ is continuous, it immediately gives

$$\left\|\boldsymbol{v}\right\|_D=\left\|\boldsymbol{v}\right\|_V.$$

Also, the symmetric positive definiteness of the tensor $\underline{\boldsymbol{D}}$ and Korn's inequality imply that

$$\left\|\nabla\boldsymbol{v}\right\|_{L_2(\Omega)}\lesssim\left\|\boldsymbol{v}\right\|_D. \tag{5.14}$$

Furthermore, it holds that $\left\|\boldsymbol{v}\right\|_D\lesssim|\boldsymbol{v}|_{H^1(\Omega)}$.

Lemma 5.1. *For any t, we have*

$$\begin{aligned}\left\|\boldsymbol{u}(t)-\boldsymbol{U}(t)\right\|_D^2 \lesssim \|\boldsymbol{u}_0-\boldsymbol{u}_{0,h}\|_{H^1(\Omega)}^2 + \left\|\boldsymbol{g}_N(t)-\boldsymbol{g}_{N,h}(t)\right\|_{L_2(\Gamma_N)}^2 + \left\|\boldsymbol{g}_N(0)-\boldsymbol{g}_{N,h}(0)\right\|_{L_2(\Gamma_N)}^2 \\ + \int_0^t \left\|\dot{\boldsymbol{g}}_N(t')-\dot{\boldsymbol{g}}_{N,h}(t')\right\|_{L_2(\Gamma_N)}^2 dt'.\end{aligned}$$

Proof. It is easy to show the argument using linearity and continuity of the solution. Let us denote $\boldsymbol{\theta}(t) = \boldsymbol{u}(t) - \boldsymbol{U}(t)$. By subtracting (5.9) from (3.2), we obtain

$$-\nabla\cdot\underline{\boldsymbol{\sigma}}(\boldsymbol{\theta}(t)) = \mathbf{0}.$$

Expanding the constitutive relation, multiplying it by $\dot{\boldsymbol{\theta}}(t)$, using the boundary conditions, and integrating over the space and the time, we can derive

$$\frac{\varphi_0}{2}\left\|\boldsymbol{\theta}(t)\right\|_D^2 - \frac{\varphi_0}{2}\left\|\boldsymbol{\theta}(0)\right\|_D^2 \le \int_0^t \left(\boldsymbol{g}_N(t')-\boldsymbol{g}_{N,h}(t'), \dot{\boldsymbol{\theta}}(t')\right)_{L_2(\Gamma_N)} dt', \tag{5.15}$$

by the positive definiteness (2.4). As seen before, using the continuous version of Trace inequality, Cauchy-Schwarz inequality, Young's inequality, and integration by parts, we can complete the proof. □

We refer to [11, 36] for the weak formulation of the continuous problem. This auxiliary problem is only required to decompose and control the errors systematically. In practice, we do not need to compute the continuous solution.

With our DG formulation, we aim to separate the error into the conforming part and the nonconforming part. Hence we define the conforming DG space by

$$\boldsymbol{\mathcal{D}}_k^c(\mathcal{E}_h) = \boldsymbol{\mathcal{D}}_k(\mathcal{E}_h) \cap \boldsymbol{H}^1(\Omega),$$

and decompose the DG finite element space as

$$\boldsymbol{\mathcal{D}}_k(\mathcal{E}_h) = \boldsymbol{\mathcal{D}}_k^c(\mathcal{E}_h) \bigoplus \boldsymbol{\mathcal{D}}_k^{\perp}(\mathcal{E}_h),$$

where $\boldsymbol{\mathcal{D}}_k^{\perp}(\mathcal{E}_h)$ is the orthogonal complement of $\boldsymbol{\mathcal{D}}_k^c(\mathcal{E}_h)$. Furthermore, we define the subspace $\mathring{\boldsymbol{\mathcal{D}}}_k^c(\mathcal{E}_h)$ of the conforming space that strongly imposes boundary conditions. As in the work of Bird et al.[21], we assume that the interpolation operator $\mathcal{I}_k : \boldsymbol{\mathcal{D}}_k(\mathcal{E}_h) \mapsto \boldsymbol{\mathcal{D}}_k^c(\mathcal{E}_h)$ satisfies that

$$h_E^{-1}\left\|\boldsymbol{v}-\mathcal{I}_k(\boldsymbol{v})\right\|_{L_2(E)} \lesssim \left\|\nabla\boldsymbol{v}\right\|_{L_2(E)}, \tag{5.16}$$

$$\left\|\nabla(\boldsymbol{v}-\mathcal{I}_k(\boldsymbol{v}))\right\|_{L_2(E)} \lesssim \left\|\nabla\boldsymbol{v}\right\|_{L_2(E)}, \tag{5.17}$$

$$|e|^{-1/2}\left\|\boldsymbol{v}-\mathcal{I}_k(\boldsymbol{v})\right\|_{L_2(e)} \lesssim \left\|\nabla\boldsymbol{v}\right\|_{L_2(E)}, \tag{5.18}$$

where $E \in \mathcal{E}_h$ and $e \subset \partial E$, for any $\boldsymbol{v} \in \boldsymbol{\mathcal{D}}_k(\mathcal{E}_h)$. Finally, we introduce the splitting form of the solution as

$$\boldsymbol{u}_h(t) - \mathcal{I}_k\boldsymbol{U}(t) := \boldsymbol{u}_h^c(t) + \boldsymbol{u}_h^r(t), \tag{5.19}$$

where $\boldsymbol{u}_h^c(t) \in \mathring{\boldsymbol{\mathcal{D}}}_k^c(\mathcal{E}_h)$ and $\boldsymbol{u}_h^r(t) \in \boldsymbol{\mathcal{D}}_k^{\perp}(\mathcal{E}_h)$. Consequently, we have

$$\begin{aligned}\left\|\boldsymbol{u}(t)-\boldsymbol{u}_h(t)\right\|_V \le& \left\|\boldsymbol{u}(t)-\boldsymbol{U}(t)\right\|_V + \left\|\boldsymbol{U}(t)-\boldsymbol{u}_h(t)\right\|_V \\ =& \left\|\boldsymbol{u}(t)-\boldsymbol{U}(t)\right\|_V + \left\|\boldsymbol{U}(t)-\mathcal{I}_k\boldsymbol{U}(t)-\boldsymbol{u}_h^c(t)-\boldsymbol{u}_h^r(t)\right\|_V \\ \le& \left\|\boldsymbol{u}(t)-\boldsymbol{U}(t)\right\|_V + \left\|\boldsymbol{U}(t)-\mathcal{I}_k\boldsymbol{U}(t)-\boldsymbol{u}_h^c(t)\right\|_V + \left\|\boldsymbol{u}_h^r(t)\right\|_V,\end{aligned} \tag{5.20}$$

by triangular inequalities and (5.19). Since $\boldsymbol{u}(t) - \boldsymbol{U}(t)$ is continuous over the spatial domain, the first term of the right hand side of (5.20) is bounded by the data oscillation term:

$$\left\|\boldsymbol{u}(t)-\boldsymbol{U}(t)\right\|_V = \left\|\boldsymbol{u}(t)-\boldsymbol{U}(t)\right\|_D \lesssim osc(t), \tag{5.21}$$

by Lemma 5.1. To complete *a posteriori* error estimate theorem, we shall show the upper bounds of the conforming and nonconforming parts, respectively.

Consider $\left\|\boldsymbol{U}(t)-\mathcal{I}_k\boldsymbol{U}(t)-\boldsymbol{u}_h^c(t)\right\|_V$. We can rewrite it as

$$\left\|\boldsymbol{U}(t)-\mathcal{I}_k\boldsymbol{U}(t)-\boldsymbol{u}_h^c(t)\right\|_V^2 = \left\|(\boldsymbol{u}(t)-\boldsymbol{u}(t)) + \boldsymbol{U}(t)-\boldsymbol{u}_h(t)+\boldsymbol{u}_h^r(t)\right\|_V^2$$

by adding zero and (5.19). Let us define $\boldsymbol{\chi}(t) \in \mathring{\boldsymbol{\mathcal{D}}}_k^c(\mathcal{E}_h)$ by

$$\boldsymbol{\chi}(t) = \frac{\boldsymbol{U}(t) - \mathcal{I}_k \boldsymbol{U}(t) - \boldsymbol{u}_h^c(t)}{\left\|\boldsymbol{U}(t) - \mathcal{I}_k \boldsymbol{U}(t) - \boldsymbol{u}_h^c(t)\right\|_V},$$

and introduce the bilinear form $b(\cdot,\cdot)$ by

$$b(\boldsymbol{v},\boldsymbol{w}) = \sum_{E\in\mathcal{E}_h} \int_E \underline{\boldsymbol{D}}\underline{\boldsymbol{\varepsilon}}(\boldsymbol{v}) : \underline{\boldsymbol{\varepsilon}}(\boldsymbol{w})\, dE + J_0^{\gamma_0,\gamma_1}(\boldsymbol{v},\boldsymbol{w}),$$

so that $b(\boldsymbol{v},\boldsymbol{v}) = \|\boldsymbol{v}\|_V^2$. Then, using linearity, we have

$$\begin{aligned}\left\|\boldsymbol{U}(t) - \mathcal{I}_k \boldsymbol{U}(t) - \boldsymbol{u}_h^c(t)\right\|_V =& b(\boldsymbol{U}(t) - \mathcal{I}_k \boldsymbol{U}(t) - \boldsymbol{u}_h^c(t), \boldsymbol{\chi}(t)) \\ =& b((\boldsymbol{u}(t) - \boldsymbol{u}(t)) + \boldsymbol{U}(t) - \boldsymbol{u}_h(t) + \boldsymbol{u}_h^r(t), \boldsymbol{\chi}(t)) \\ =& b(\boldsymbol{u}(t) - \boldsymbol{u}_h(t), \chi(t)) + b(\boldsymbol{U}(t) - \boldsymbol{u}(t)), \boldsymbol{\chi}(t)) + b(\boldsymbol{u}_h^r(t), \boldsymbol{\chi}(t)). \end{aligned} \tag{5.22}$$

Noting that $\left\|\boldsymbol{\chi}(t)\right\|_V = 1$, the Cauchy-Schwarz inequality and (5.21) lead to the bound

$$b(\boldsymbol{U}(t) - \boldsymbol{u}(t)), \boldsymbol{\chi}(t)) \le \left\|\boldsymbol{u}(t) - \boldsymbol{U}(t))\right\|_V \left\|\boldsymbol{\chi}(t)\right\|_V \lesssim osc(t). \tag{5.23}$$

In a similar way, we obtain

$$b(\boldsymbol{u}_h^r(t), \boldsymbol{\chi}(t)) \le \left\|\boldsymbol{u}_h^r(t)\right\|_V. \tag{5.24}$$

In the following lemma, we show the bound for the nonconforming part.

Lemma 5.2. *Let $\boldsymbol{u}_h(t)$ be the solution to* (3.7) *and $\boldsymbol{u}_h^r(t)$ be its nonconforming part. Then we have*

$$\left\|\boldsymbol{u}_h^c(t)\right\|_V \lesssim \eta_{err}(t).$$

Proof. First, let us recall the work of Karakashian and Pascal [42] to define a projection operator $\pi_k : \boldsymbol{\mathcal{D}}_k(\mathcal{E}_h) \mapsto \mathring{\boldsymbol{\mathcal{D}}}_k^c(\mathcal{E}_h)$. The projection operator satisfies the following property:

$$\sum_{E\in\mathcal{E}_h} \left\|\nabla(\boldsymbol{v} - \pi_k \boldsymbol{v})\right\|_{L_2(E)}^2 \lesssim \sum_{e\subset\Gamma_h\cup\Gamma_D} |e|^{-1} \int_e |[\boldsymbol{v}]|^2 de, \qquad \forall \boldsymbol{v} \in \boldsymbol{\mathcal{D}}_k(\mathcal{E}_h). \tag{5.25}$$

We refer to [42, Theorem 2.1] for more detail and to [21] for the extended application.

We note that the decomposition of the solution implies $[\boldsymbol{u}_h(t)] = [\boldsymbol{u}_h^r(t)]$ on the interior edges. Hence, we have

$$\left\|\boldsymbol{u}_h^r(t)\right\|_V^2 = \sum_{E\in\mathcal{E}_h} \int_E \underline{\boldsymbol{D}}\underline{\boldsymbol{\varepsilon}}(\boldsymbol{u}_h^r(t)) : \underline{\boldsymbol{\varepsilon}}(\boldsymbol{u}_h^r(t)) dE + J_0^{\gamma_0,\gamma_1}(\boldsymbol{u}_h(t), \boldsymbol{u}_h(t)). \tag{5.26}$$

It is obvious that

$$J_0^{\gamma_0,\gamma_1}(\boldsymbol{u}_h(t), \boldsymbol{u}_h(t)) \lesssim \sum_{E\in\mathcal{E}_h} \eta_{2,E}^2(t).$$

For any $\boldsymbol{v}^r \in \boldsymbol{\mathcal{D}}_k^{\perp}(\mathcal{E}_h)$, we can denote $\boldsymbol{v}^r = \boldsymbol{v} - \pi_k \boldsymbol{v}$ for some $\boldsymbol{v} \in \boldsymbol{\mathcal{D}}_k(\mathcal{E}_h)$. Therefore, (5.25) implies that

$$\sum_{E\in\mathcal{E}_h} \int_E \underline{\boldsymbol{D}}\underline{\boldsymbol{\varepsilon}}(\boldsymbol{u}_h^r(t)) : \underline{\boldsymbol{\varepsilon}}(\boldsymbol{u}_h^r(t)) dE \lesssim \sum_{e\subset\Gamma_h\cup\Gamma_D} |e|^{-1} \int_e |[\boldsymbol{u}_h(t)]|^2 de \lesssim \sum_{E\in\mathcal{E}_h} \eta_{2,E}^2(t), \tag{5.27}$$

since $\underline{\boldsymbol{D}}$ is symmetric positive definite. Consequently, we derive

$$\left\|\boldsymbol{u}_h^c(t)\right\|_V \lesssim \eta_{\text{err}}(t).$$

□

Lastly, we focus on the bound of the remaining term $b(\boldsymbol{u}(t) - \boldsymbol{u}_h(t), \boldsymbol{\chi}(t))$. Recall the semi-discrete problem (3.7) and define $\tilde{B}$ such that $\tilde{B}(\boldsymbol{v},\boldsymbol{w}) = a(\boldsymbol{v},\boldsymbol{w}) - b(\boldsymbol{v},\boldsymbol{w})$ corresponding to interior penalty terms. As $\boldsymbol{u}(t)$ is the strong solution to (3.3), we have

$$\varphi_0 b(\boldsymbol{u}(t) - \boldsymbol{u}_h(t), \boldsymbol{v}) + \varphi_\alpha b\left({}_0I_t^{1-\alpha}(\dot{\boldsymbol{u}}(t) - \dot{\boldsymbol{u}}_h(t)), \boldsymbol{v}\right) = \boldsymbol{F}(t;\boldsymbol{v}) - \varphi_0 b(\boldsymbol{u}_h(t), \boldsymbol{v}) - \varphi_\alpha b\left({}_0I_t^{1-\alpha}\dot{\boldsymbol{u}}_h(t), \boldsymbol{v}\right), \tag{5.28}$$

for any $\boldsymbol{v} \in \mathring{\boldsymbol{\mathcal{D}}}_k^c(\mathcal{E}_h)$. Since, from (3.7),

$$\boldsymbol{F}(t;\boldsymbol{v}_h) - \varphi_0 b\left(\boldsymbol{u}_h(t),\boldsymbol{v}_h\right) - \varphi_\alpha b\left({}_0I_t^{1-\alpha}\dot{\boldsymbol{u}}_h(t),\boldsymbol{v}_h\right) - \varphi_0\tilde{B}\left(\boldsymbol{u}_h(t),\boldsymbol{v}_h\right) - \varphi_\alpha\tilde{B}\left({}_0I_t^{1-\alpha}\dot{\boldsymbol{u}}_h(t),\boldsymbol{v}_h\right) = \boldsymbol{0},$$

where $\boldsymbol{v}_h \in \boldsymbol{\mathcal{D}}_k(\mathcal{E}_h)$, adding zero into (5.28) gives

$$\begin{aligned}\varphi_0 b\left(\boldsymbol{u}(t)-\boldsymbol{u}_h(t),\boldsymbol{v}\right) + \varphi_\alpha b\left({}_0I_t^{1-\alpha}(\dot{\boldsymbol{u}}(t)-\dot{\boldsymbol{u}}_h(t)),\boldsymbol{v}\right) =& \boldsymbol{F}(t;\boldsymbol{v}-\boldsymbol{v}_h) - \varphi_0 b\left(\boldsymbol{u}_h(t),\boldsymbol{v}-\boldsymbol{v}_h\right) - \varphi_\alpha b\left({}_0I_t^{1-\alpha}\dot{\boldsymbol{u}}_h(t),\boldsymbol{v}-\boldsymbol{v}_h\right)\\ &+ \varphi_0\tilde{B}\left(\boldsymbol{u}_h(t),\boldsymbol{v}_h\right) + \varphi_\alpha\tilde{B}\left({}_0I_t^{1-\alpha}\dot{\boldsymbol{u}}_h(t),\boldsymbol{v}_h\right). \end{aligned} \tag{5.29}$$

Using this relation, we provide the following lemma.

Lemma 5.3. *Let $\boldsymbol{u}(t)$ and $\boldsymbol{u}_h(t)$ be the exact and the semi-discrete problem, respectively. For any continuous $\boldsymbol{v}$ subject to homogeneous Dirichlet boundary condition on Γ_D, it holds that*

$$b\left(\boldsymbol{u}(t)-\boldsymbol{u}_h(t),\boldsymbol{v}\right) + b\left({}_0I_t^{1-\alpha}(\dot{\boldsymbol{u}}(t)-\dot{\boldsymbol{u}}_h(t)),\boldsymbol{v}\right) \lesssim \left(\eta_{err}(t) + osc(t)\right)\left\|\boldsymbol{v}\right\|_V.$$

Proof. Consider (5.29) with letting $\boldsymbol{\varpi}_h(t) = \varphi_0\boldsymbol{u}_h(t) + \varphi_{\alpha 0}I_t^{1-\alpha}\dot{\boldsymbol{u}}_h(t)$. Note that

$$\underline{\boldsymbol{\sigma}}(\boldsymbol{u}_h(t)) = \underline{\boldsymbol{D}}\underline{\boldsymbol{\varepsilon}}(\boldsymbol{\varpi}_h(t)).$$

Hence, by integration by parts and the Leibniz integral rule, we have

$$\begin{aligned}\boldsymbol{F}(t;\boldsymbol{v}-\boldsymbol{v}_h) - b\left(\boldsymbol{\varpi}_h(t),\boldsymbol{v}-\boldsymbol{v}_h\right) + \tilde{B}\left(\boldsymbol{\varpi}_h(t),\boldsymbol{v}_h\right) =& \boldsymbol{F}(t;\boldsymbol{v}-\boldsymbol{v}_h) + \sum_{E\in\mathcal{E}_h}\int_E \nabla\cdot\underline{\boldsymbol{\sigma}}(\boldsymbol{u}_h(t))\cdot(\boldsymbol{v}-\boldsymbol{v}_h)dE\\ &- J_0^{\gamma_0,\gamma_1}\left(\boldsymbol{\varpi}_h(t),\boldsymbol{v}-\boldsymbol{v}_h\right)\\ &- \sum_{E\in\mathcal{E}_h}\int_{\partial E}\underline{\boldsymbol{\sigma}}(\boldsymbol{u}_h(t)) : (\boldsymbol{v}-\boldsymbol{v}_h)\otimes\boldsymbol{n}_e de + \tilde{B}\left(\boldsymbol{\varpi}_h(t),\boldsymbol{v}_h\right), \end{aligned} \tag{5.30}$$

where $\boldsymbol{v}_h = \mathcal{I}_k\boldsymbol{v}$. By the spatial continuity of $\boldsymbol{v}$, it yields

$$\begin{aligned}&\tilde{B}\left(\boldsymbol{\varpi}_h(t),\boldsymbol{v}_h\right) - \sum_{E\in\mathcal{E}_h}\int_{\partial E}\underline{\boldsymbol{\sigma}}(\boldsymbol{u}_h(t)) : (\boldsymbol{v}-\boldsymbol{v}_h)\otimes\boldsymbol{n}_e de\\ =& -\sum_{e\subset\Gamma_h\cup\Gamma_D}\int_e[\boldsymbol{\varpi}_h(t)\otimes\boldsymbol{n}_e] : \{\underline{\boldsymbol{D}}\underline{\boldsymbol{\varepsilon}}(\boldsymbol{v}_h)\}de - \sum_{e\subset\partial\Omega}\int_e\underline{\boldsymbol{\sigma}}(\boldsymbol{u}_h(t)) : (\boldsymbol{v}-\boldsymbol{v}_h)\otimes\boldsymbol{n}_e de\\ &- \sum_{e\subset\Gamma_h}\int_e[\underline{\boldsymbol{\sigma}}(\boldsymbol{u}_h(t))] : \{(\boldsymbol{v}-\boldsymbol{v}_h)\otimes\boldsymbol{n}_e\}de - \sum_{e\subset\Gamma_D}\int_e\underline{\boldsymbol{\sigma}}(\boldsymbol{u}_h(t)) : \boldsymbol{v}_h\otimes\boldsymbol{n}_e de\\ =& -\sum_{e\subset\Gamma_h\cup\Gamma_D}\int_e[\boldsymbol{\varpi}_h(t)\otimes\boldsymbol{n}_e] : \{\underline{\boldsymbol{D}}\underline{\boldsymbol{\varepsilon}}(\boldsymbol{v}_h)\}de - \sum_{e\subset\Gamma_N}\int_e\underline{\boldsymbol{\sigma}}(\boldsymbol{u}_h(t)) : (\boldsymbol{v}-\boldsymbol{v}_h)\otimes\boldsymbol{n}_e de\\ &- \sum_{e\subset\Gamma_h}\int_e[\underline{\boldsymbol{\sigma}}(\boldsymbol{u}_h(t))] : \{(\boldsymbol{v}-\boldsymbol{v}_h)\otimes\boldsymbol{n}_e\}de - \sum_{e\subset\Gamma_D}\int_e\underline{\boldsymbol{\sigma}}(\boldsymbol{u}_h(t)) : \boldsymbol{v}\otimes\boldsymbol{n}_e de, \end{aligned} \tag{5.31}$$

since

$$\begin{aligned}&\sum_{E\in\mathcal{E}_h}\int_{\partial E}\underline{\boldsymbol{\sigma}}(\boldsymbol{u}_h(t)) : (\boldsymbol{v}-\boldsymbol{v}_h)\otimes\boldsymbol{n}_e de\\ &= \sum_{e\subset\partial\Omega}\int_e\underline{\boldsymbol{\sigma}}(\boldsymbol{u}_h(t)) : (\boldsymbol{v}-\boldsymbol{v}_h)\otimes\boldsymbol{n}_e de + \sum_{e\subset\Gamma_h}\int_e[\underline{\boldsymbol{\sigma}}(\boldsymbol{u}_h(t))] : \{(\boldsymbol{v}-\boldsymbol{v}_h)\otimes\boldsymbol{n}_e\}de\\ &\quad - \sum_{e\subset\Gamma_h}\int_e\{\underline{\boldsymbol{\sigma}}(\boldsymbol{u}_h(t))\} : [\boldsymbol{v}_h\otimes\boldsymbol{n}_e]de. \end{aligned}$$

Combining with (5.30) and (5.31), (5.29) can be rewritten as

$$\begin{aligned}&\varphi_0 b\left(\boldsymbol{u}(t)-\boldsymbol{u}_h(t),\boldsymbol{v}\right) + \varphi_\alpha b\left({}_0I_t^{1-\alpha}(\dot{\boldsymbol{u}}(t)-\dot{\boldsymbol{u}}_h(t)),\boldsymbol{v}\right)\\ &= (\boldsymbol{f}(t),\boldsymbol{v}-\boldsymbol{v}_h) + \sum_{E\in\mathcal{E}_h}\int_E\nabla\cdot\underline{\boldsymbol{\sigma}}(\boldsymbol{u}_h(t))\cdot(\boldsymbol{v}-\boldsymbol{v}_h)dE - J_0^{\gamma_0,\gamma_1}\left(\boldsymbol{\varpi}_h(t),\boldsymbol{v}-\boldsymbol{v}_h\right)\end{aligned}$$

$$- \sum_{e\subset\Gamma_h\cup\Gamma_D}\int_e [\boldsymbol{\varpi}_h(t)\otimes\boldsymbol{n}_e] : \{\underline{\boldsymbol{D}}\underline{\boldsymbol{\varepsilon}}(\boldsymbol{v}_h)\}de + (\boldsymbol{g}_N(t),\boldsymbol{v}-\boldsymbol{v}_h)_{L_2(\Gamma_N)} - \sum_{e\subset\Gamma_N}\int_e \underline{\boldsymbol{\sigma}}(\boldsymbol{u}_h(t)) : (\boldsymbol{v}-\boldsymbol{v}_h)\otimes\boldsymbol{n}_e de$$
$$- \sum_{e\subset\Gamma_h}\int_e [\underline{\boldsymbol{\sigma}}(\boldsymbol{u}_h(t))] : \{(\boldsymbol{v}-\boldsymbol{v}_h)\otimes\boldsymbol{n}_e\}de - \sum_{e\subset\Gamma_D}\int_e \underline{\boldsymbol{\sigma}}(\boldsymbol{u}_h(t)) : \boldsymbol{v}\otimes\boldsymbol{n}_e de. \tag{5.32}$$

Next, we will determine the bounds for each term on the right hand side of (5.32):

- $(\boldsymbol{f}(t),\boldsymbol{v}-\boldsymbol{v}_h) + \sum_{E\in\mathcal{E}_h}\int_E \nabla\cdot\underline{\boldsymbol{\sigma}}(\boldsymbol{u}_h(t))\cdot(\boldsymbol{v}-\boldsymbol{v}_h)dE$
  Using the Cauchy-Schwarz inequality and (5.16) gives that

$$\begin{aligned}
&(\boldsymbol{f}(t),\boldsymbol{v}-\boldsymbol{v}_h) + \sum_{E\in\mathcal{E}_h}\int_E \nabla\cdot\underline{\boldsymbol{\sigma}}(\boldsymbol{u}_h(t))\cdot(\boldsymbol{v}-\boldsymbol{v}_h)dE\\
&= \sum_{E\in\mathcal{E}_h}\int_E (\boldsymbol{f}(t)-\boldsymbol{f}_h(t))\cdot(\boldsymbol{v}-\boldsymbol{v}_h)dE + \sum_{E\in\mathcal{E}_h}\int_E (\boldsymbol{f}_h(t)-\nabla\cdot\underline{\boldsymbol{\sigma}}(\boldsymbol{u}_h(t)))\cdot(\boldsymbol{v}-\boldsymbol{v}_h)dE\\
&\le \sum_{E\in\mathcal{E}_h}\left\|\boldsymbol{f}(t)-\boldsymbol{f}_h(t)\right\|_{L_2(E)}\left\|\boldsymbol{v}-\boldsymbol{v}_h\right\|_{L_2(E)} + \sum_{E\in\mathcal{E}_h}\left\|\boldsymbol{f}_h(t)-\nabla\cdot\underline{\boldsymbol{\sigma}}(\boldsymbol{u}_h(t))\right\|_{L_2(E)}\left\|\boldsymbol{v}-\boldsymbol{v}_h\right\|_{L_2(E)}\\
&\le \left(\sum_{E\in\mathcal{E}_h} h_E^2\left\|\boldsymbol{f}(t)-\boldsymbol{f}_h(t)\right\|_{L_2(E)}^2\right)^{1/2}\left(\sum_{E\in\mathcal{E}_h} h_E^{-2}\left\|\boldsymbol{v}-\boldsymbol{v}_h\right\|_{L_2(E)}^2\right)^{1/2}\\
&\quad + \left(\sum_{E\in\mathcal{E}_h} h_E^2\left\|\boldsymbol{f}_h(t)-\nabla\cdot\underline{\boldsymbol{\sigma}}(\boldsymbol{u}_h(t))\right\|_{L_2(E)}^2\right)^{1/2}\left(\sum_{E\in\mathcal{E}_h} h_E^{-2}\left\|\boldsymbol{v}-\boldsymbol{v}_h\right\|_{L_2(E)}^2\right)^{1/2}\\
&\lesssim \left(\left(\sum_{E\in\mathcal{E}_h}\eta_{1,E}^2(t)\right)^{1/2} + \left(\sum_{E\in\mathcal{E}_h} osc_{2,E}^2(t)\right)^{1/2}\right)\left\|\boldsymbol{v}\right\|_V.
\end{aligned}$$

- $-J_0^{\gamma_0,\gamma_1}(\boldsymbol{\varpi}_h(t),\boldsymbol{v}-\boldsymbol{v}_h)$
  As seen before, we employ the Cauchy-Schwarz inequality and (5.18) to derive

$$-J_0^{\gamma_0,\gamma_1}(\boldsymbol{\varpi}_h(t),\boldsymbol{v}-\boldsymbol{v}_h) \lesssim \left(\sum_{E\in\mathcal{E}_h}\eta_{2,E}^2(t)\right)^{1/2}\left\|\boldsymbol{v}\right\|_V.$$

- $-\sum_{e\subset\Gamma_h\cup\Gamma_D}\int_e[\boldsymbol{\varpi}_h(t)\otimes\boldsymbol{n}_e] : \{\underline{\boldsymbol{D}}\underline{\boldsymbol{\varepsilon}}(\boldsymbol{v}_h)\}de$
  By applying the Cauchy-Schwarz inequality, the trace inequality and (5.17), we can obtain

$$-\sum_{e\subset\Gamma_h\cup\Gamma_D}\int_e[\boldsymbol{\varpi}_h(t)\otimes\boldsymbol{n}_e] : \{\underline{\boldsymbol{D}}\underline{\boldsymbol{\varepsilon}}(\boldsymbol{v}_h)\}de \lesssim \left(\sum_{E\in\mathcal{E}_h}\eta_{2,E}^2(t)\right)^{1/2}\left\|\boldsymbol{v}\right\|_V.$$

- $(\boldsymbol{g}_N(t),\boldsymbol{v}-\boldsymbol{v}_h)_{L_2(\Gamma_N)} - \sum_{e\subset\Gamma_N}\int_e \underline{\boldsymbol{\sigma}}(\boldsymbol{u}_h(t))\cdot\boldsymbol{n}_e\cdot(\boldsymbol{v}-\boldsymbol{v}_h)de$
  By adding zero and rearranging the equation, we have

$$\begin{aligned}
&(\boldsymbol{g}_N(t),\boldsymbol{v}-\boldsymbol{v}_h)_{L_2(\Gamma_N)} - \sum_{e\subset\Gamma_N}\int_e \underline{\boldsymbol{\sigma}}(\boldsymbol{u}_h(t)) : (\boldsymbol{v}-\boldsymbol{v}_h)\otimes\boldsymbol{n}_e de\\
&= (\boldsymbol{g}_N(t),\boldsymbol{v}-\boldsymbol{v}_h)_{L_2(\Gamma_N)} - \sum_{e\subset\Gamma_N}\int_e \underline{\boldsymbol{\sigma}}(\boldsymbol{u}_h(t))\cdot\boldsymbol{n}_e\cdot(\boldsymbol{v}-\boldsymbol{v}_h)de\\
&= \sum_{e\subset\Gamma_N}\int_e(\boldsymbol{g}_N(t)-\boldsymbol{g}_{N,h}(t))\cdot(\boldsymbol{v}-\boldsymbol{v}_h)de - \sum_{e\subset\Gamma_N}\int_e\left(\underline{\boldsymbol{\sigma}}(\boldsymbol{u}_h(t))\cdot\boldsymbol{n}_e-\boldsymbol{g}_{N,h}(t)\right)\cdot(\boldsymbol{v}-\boldsymbol{v}_h)de,
\end{aligned}$$

  hence the use of the Cauchy-Schwarz inequality, the trace inequality and (5.17) immediately implies that

$$(\boldsymbol{g}_N(t),\boldsymbol{v}-\boldsymbol{v}_h)_{L_2(\Gamma_N)} - \sum_{e\subset\Gamma_N}\int_e \underline{\boldsymbol{\sigma}}(\boldsymbol{u}_h(t)) : (\boldsymbol{v}-\boldsymbol{v}_h)\otimes\boldsymbol{n}_e de$$

$$\lesssim \left(\left(\sum_{E \in \mathcal{E}_h} \eta_{3,E}^2(t) \right)^{1/2} + \left(\sum_{E \in \mathcal{E}_h} osc_{3,E}^2(t) \right)^{1/2} \right) \|\boldsymbol{v}\|_V.$$

- $-\sum_{e \subset \Gamma_h} \int_e [\underline{\boldsymbol{\sigma}}(\boldsymbol{u}_h(t))] : \{(\boldsymbol{v} - \boldsymbol{v}_h) \otimes \boldsymbol{n}_e\} de$
  In the same manner in the previous bounds, we have

$$-\sum_{e \subset \Gamma_h} \int_e [\underline{\boldsymbol{\sigma}}(\boldsymbol{u}_h(t))] : \{(\boldsymbol{v} - \boldsymbol{v}_h) \otimes \boldsymbol{n}_e\} de \lesssim \left(\sum_{E \in \mathcal{E}_h} \eta_{3,E}^2(t) \right)^{1/2} \|\boldsymbol{v}\|_V.$$

- $-\sum_{e \subset \Gamma_D} \int_e \underline{\boldsymbol{\sigma}}(\boldsymbol{u}_h(t)) : \boldsymbol{v} \otimes \boldsymbol{n}_e de$
  Due to the homogeneous boundary condition of $\boldsymbol{v}$, it straightforwardly gives

$$-\sum_{e \subset \Gamma_D} \int_e \underline{\boldsymbol{\sigma}}(\boldsymbol{u}_h(t)) : \boldsymbol{v} \otimes \boldsymbol{n}_e de = 0.$$

Tidying up all the results, we complete the proof. □

Remark 4. *To obtain the bound of $b(\boldsymbol{u}(t) - \boldsymbol{u}_h(t), \boldsymbol{\chi}(t))$, we set $\boldsymbol{v} = \boldsymbol{\chi}(t)$ in Lemma 5.3. For any t, since $\|\boldsymbol{\chi}(t)\|_V = 1$, the upper bound can be derived.*

Finally, we have the following *a posteriori* error estimate theorem.

Theorem 5.1. *Let $\boldsymbol{u}$ and $\boldsymbol{u}_h$ be the exact and semi-discrete solution of our model problem. Then, it holds that*

$$\|\boldsymbol{u} - \boldsymbol{u}_h\|_{L_\infty(0,T;V)} \lesssim \|\eta_{err}\|_{L_\infty(0,T)} + \|osc\|_{L_\infty(0,T)}.$$

Proof. The proof can be done by splitting the error as in (5.20), constructing the upper bounds from (5.21), (5.22), (5.23), (5.24) with Lemma 5.2 and 5.3, and taking into account L_∞ norm in time. □

For the *a posteriori* estimates in the fully discrete case, temporal errors must also be taken into account. Due to space limitations, we provide only a brief description and outline of the analysis for the fully discrete problem.

As in the semi-discrete case, the Scott-Zhang-type reconstruction [43, 44] is required for the spatial component. For the temporal part, such methods like elliptic reconstruction [45, 41] are commonly used in parabolic problems. However, elliptic reconstruction is not applicable to fractional-order integro-differential equations. Recently, Banjai and Makridakis [24] provided an *a posteriori* error analysis for time-fractional subdiffusion problems with pointwise representations. Their approach yields optimal *a posteriori* error estimates, though their discrete scheme achieves only a $1 + \alpha$ order of convergence in time in the *a priori* analysis.

In contrast, our numerical scheme introduces a discrete velocity via the Crank-Nicolson method, achieving second-order accuracy. Hence, a simple temporal linear reconstruction is inadequate for our approach. Instead, to handle the hereditary term in the fractional integral, the Ritz-Volterra reconstruction [46, 47] is more appropriate for establishing temporal components with memory effects. However, due to the weak singularity of our kernel, a modified Ritz-Volterra reconstruction is necessary-potentially combined with Crank-Nicolson reconstruction [48].

Remark 5. *This paper does not address p- (polynomial degrees, denoted by k in our work) or hp-adaptivity in DG methods. For simplicity, our discretization assumes a quasi-uniform mesh, uniform time discretization and a constant polynomial degree. However, the techniques and analysis presented here can be extended to the hp-adaptive DGFEM framework without loss of generality. The additional complexities arising from varying mesh sizes h and polynomial degrees p can be introduced in our error estimates with appropriate modifications. Variable time stepping can also be employed. For a more comprehensive treatment of hp-adaptivity and related theoretical results, we refer the reader to standard works such as Melenk [43], Houston et al. [20], and Bird et al. [21].*

6 Numerical experiments

In this section, we present a series of numerical experiments designed to validate our proposed DGFEM for quasi-static viscoelastic problems characterized by fractional-order behavior. Our primary objectives are to assess the accuracy of the method,

investigate convergence rates, and demonstrate our error analysis. To conduct these experiments, we utilized the finite element method library FEniCS[1] of version 2019.1.0, a robust computational framework that facilitates the implementation of our numerical method. This tool enables efficient handling of the complexities associated with fractional-order viscoelasticity, providing a reliable environment for testing our approach. The numerical simulations discussed in this paper were carried out using code that can be found in the author's GitHub repository[2]. We emphasize the importance of open and reproducible research, encouraging readers to examine our code for a deeper insight into the proposed methodology.

We consider two test cases: the first involves a user-defined exact solution that meets the regularity conditions outlined in the error estimate theorem. This allows us to analyze the convergence and accuracy of our approach in a controlled setting. The second test case utilizes real-material data, providing a practical context to assess the applicability of our methods to actual viscoelastic problems. Through these experiments, we demonstrate the effectiveness and robustness of our numerical framework.

Define the numerical error as $\boldsymbol{e}^n := \boldsymbol{u}(t_n) - \boldsymbol{U}_h^n$. Given that the DG energy norm relies on the penalty parameters γ_0 and γ_1, we instead consider the H^1 norm of the errors. By Korn's inequality, we can derive error estimates in the H^1 norm that exhibits the same convergence rates as those obtained from the DG energy error estimates. Consequently, according to Theorem 4.4, for a solution possessing H^3 regularity in time, along with adequately smooth functions for $\boldsymbol{f}$ and the initial conditions, the error estimates are as follows $\forall n$:

$$\|\boldsymbol{e}^n\|_{H^1(\Omega)} = O(h^{r-1} + \Delta t^2) \qquad \text{and} \qquad \left\|\boldsymbol{e}^n\right\|_{L_2(\Omega)} = O(h^r + \Delta t^2).$$

Here, $r = \min(k+1, s)$ represents the spatial convergence rate, α denotes the fractional order of the time derivative, and h and Δt refer to the mesh sizes in spatial and temporal spaces, respectively. The numerical convergence rate can be calculated by taking the logarithmic difference between two error values divided by the logarithmic difference in the corresponding mesh sizes.

To ensure the stability of our numerical scheme, it is essential to select sufficiently large penalty parameters. The coercivity, continuity, DG elliptic error estimates, and bounds for the interior penalty are all dependent on these parameters. For an illustration of the issues that can arise in DG simulations when penalty parameters are inadequate, we refer the reader to [36]. In the subsequent numerical experiments, we set $\gamma_0 = 20$ and $\gamma_1 = 1$ for the 2D problems.

While we present the *a posteriori* error estimator of the semi-discrete problem, we introduce and compute the following error estimator of fully discrete variant:

$$\begin{aligned}\eta^n := \sum_{E\in\mathcal{E}_h} \Bigg(& h_E^2 \left\| \boldsymbol{f}_h(t_n) + \nabla\cdot\underline{\boldsymbol{D}}\,\underline{\boldsymbol{\varepsilon}}(\boldsymbol{U}_h^n) + \nabla\cdot\underline{\boldsymbol{D}}\,\underline{\boldsymbol{\varepsilon}}(\boldsymbol{Q}_n(\boldsymbol{W}_h)) \right\|_{L_2(E)}^2 + \sum_{e\subset\partial E\cap(\Gamma_h\cup\Gamma_D)} |e|^{-1} \left(\left\| [\boldsymbol{U}_h^n + \boldsymbol{Q}_n(\boldsymbol{W}_h)] \right\|_{L_2(e)}^2 \right) \\ & + \sum_{e\subset\partial E\cap\Gamma_h} |e| \left\| [\underline{\boldsymbol{D}}\,\underline{\boldsymbol{\varepsilon}}(\boldsymbol{U}_h^n) + \underline{\boldsymbol{D}}\,\underline{\boldsymbol{\varepsilon}}(\boldsymbol{Q}_n(\boldsymbol{W}_h))] \right\|_{L_2(e)}^2 \\ & + \sum_{e\subset\partial E\cap\Gamma_N} |e| \left\| \underline{\boldsymbol{D}}\,\underline{\boldsymbol{\varepsilon}}(\boldsymbol{U}_h^n)\cdot\boldsymbol{n}_e + \underline{\boldsymbol{D}}\,\underline{\boldsymbol{\varepsilon}}(\boldsymbol{Q}_n(\boldsymbol{W}_h))\cdot\boldsymbol{n}_e - \boldsymbol{g}_{N,h}(t) \right\|_{L_2(e)}^2 \Bigg)^{1/2}. \end{aligned} \tag{6.1}$$

The error estimator (6.1) does not include a temporal error. Nevertheless, in our a posteriori error estimation, we focus primarily on the spatial discretization error. This choice is justified by the quasi-static nature of the problem and the sufficiently small time step size used in our numerical experiments. In quasi-static problems, the time evolution is slow enough that temporal variations are relatively small. This reduces the significance of the temporal error, making the total error dominated by the spatial error. Thus, the spatial error estimator provides a reliable measure of the total error in our computations.

6.1 Validation with analytical solution

Let us consider an exact solution to the primal model problem in the strong form defined by

$$\boldsymbol{u}(t,x,y) = (1+t^4) \begin{bmatrix} \sin(\pi x)\sin(\pi y) \\ x(1-x)y(1-y) \end{bmatrix} \qquad \text{on } [0,T]\times\Omega,$$

with $T = 0.01$, $\Omega = (0,1)^2$ and its boundary splitting in $\Gamma_N := \{(x,y)\in\partial\Omega \mid x = 0\}$ and $\Gamma_D := \partial\Omega\backslash\Gamma_N$. We set $\alpha = 1/2$, $\varphi_0 = 1$, $\varphi_1 = 1/\Gamma(1/2)$ and $\underline{\boldsymbol{D}}\,\underline{\boldsymbol{\varepsilon}} = \underline{\boldsymbol{\varepsilon}}$ so that $\boldsymbol{u}$ solves

$$-\nabla\cdot\dot{\underline{\boldsymbol{\varepsilon}}}(t) - \nabla\cdot {}_0I_t^{1/2}\dot{\underline{\boldsymbol{\varepsilon}}}(t) = \boldsymbol{f}(t), \tag{6.2}$$

[1] `https://fenicsproject.org`

[2] `https://github.com/Yongseok7717/quasi_visco_frac_dg`

for some $\boldsymbol{f}$ that can be readily determined analytically. Also, the traction $\boldsymbol{g}_N$ can be obtained from the exact solution. We note that the computation of fractional integrals of polynomials is easily obtained in algebra, for example, ${}_0I_t^{1/2}t^k = \Gamma(k+1)/\Gamma(k+3/2)t^{k+1/2}$. Here, we have the sufficiently smooth solution and data terms.

Let N denote the number of time stepping. Then we define the time step size Δt by T/N. For the spatial discretization, we use the uniform right-triangle meshes with $h = 1/N$. Therefore, N also indicates the number of subdivision where the total number of triangle is $2N^2$.

Table 1: Numerical errors and convergence orders with $k = 1$.

	H_1 norm error		L_2 norm error		*a posteriori* error estimator	
N	$\left\|\boldsymbol{e}^N\right\|_{H^1(\Omega)}$	Rate	$\left\|\boldsymbol{e}^N\right\|_{L_2(\Omega)}$	Rate	η^N	Rate
8	3.238e-01		5.225e-03		1.035e-00	
16	1.627e-01	0.99	1.318e-03	1.99	5.295e-01	0.97
32	8.146e-02	1.00	3.305e-04	2.00	2.672e-01	0.99
64	4.074e-02	1.00	8.272e-05	2.00	1.341e-01	0.99
128	2.037e-02	1.00	2.069e-05	2.00	6.719e-01	1.00

Table 2: Numerical errors and convergence orders with $k = 2$.

	H_1 norm error		L_2 norm error		*a posteriori* error estimator	
N	$\left\|\boldsymbol{e}^N\right\|_{H^1(\Omega)}$	Rate	$\left\|\boldsymbol{e}^N\right\|_{L_2(\Omega)}$	Rate	η^N	Rate
8	2.791e-02		2.771e-04		8.306e-02	
16	7.016e-03	1.99	3.478e-05	2.99	2.080e-02	2.00
32	1.757e-03	2.00	4.351e-06	3.00	5.211e-03	2.00
64	4.394e-04	2.00	5.441e-07	3.00	1.305e-03	2.00
128	1.099e-04	2.00	6.802e-08	3.00	3.265e-04	2.00

Tables 1 and 2 present the numerical errors, *a posteriori* errors and numerical convergent orders for linear and quadratic polynomial bases, respectively. When $k = 1$, we observe the optimal convergence rates, specifically $d = 1$ in the H_1 norm and $d = 2$ in the L_2 norm. Since the temporal error is small enough in our experiments, even the L_2 norm errors with the quadratic polynomial bases exhibit the third order accuracy. Furthermore, as seen in the tables, the error estimator η^N provides reliable values approximating the energy norm errors with the optimal order of convergence. These numerical results clearly validate the *a priori* and *a posteriori* error estimates established in our theoretical analysis.

6.2 Quasi-static viscoelasticity of butyl rubber

Based on the real material data for butyl rubber (*Butyl 70821*) from [49], we demonstrate the behavior of quasi-static fractional-order viscoelasticity for butyl rubber in a 2D setting. The material parameters are given as $\alpha = 0.449$, $\varphi_0 = 0.685\,\mathrm{MN\,m^{-2}}$, $\varphi_1 = 1.37\,\mathrm{MN\,m^{-2}}$, $\mu = 0.228$ and $\lambda = 0.456$.

We define the spatial domain as $\Omega = (0,2) \times (0,1)$. Both the initial conditions are assumed to be zero. The boundary conditions are specified as follows: the Dirichlet boundary is $\Gamma_D = \{(x,y) \in \partial\Omega \mid x = 0 \text{ or } x = 2\}$ and the Neumann boundary is $\Gamma_N = \partial\Omega \backslash \Gamma_D$. Homogeneous boundary conditions are applied on the Dirichlet boundary Γ_D (the left and right edge) and on the Neumann boundaries along the top and bottom edges. The body force $\boldsymbol{f}$ is given by

$$\boldsymbol{f}(t) = \begin{bmatrix} \mathcal{F} \\ 0 \end{bmatrix} \qquad \forall\, t,$$

where $\mathcal{F} = 1\,\mathrm{MN\,m^{-2}}$. Thus, the system is subject to a constant body force, and homogeneous Dirichlet and Neumann boundary condition.

With the initial condition and boundary conditions, our discrete scheme ensures the stability. Consequently, if the exact solution possesses sufficient regularity, the numerical solution will satisfy the *a priori* error estimates. As the exact solution is unavailable, direct computation of error norms cannot be carried out, but we are able to provide *a posteriori* error estimates. To highlight the differences between elastic and viscoelastic mechanical responses, we additionally solve a linear elastic model by setting $\varphi_1 = 0$, for simplicity. The constitutive equation of the linear elasticity model is given by $\underline{\boldsymbol{\sigma}}_{\text{elastic}}(t) = \varphi_0 \underline{\boldsymbol{D}}\underline{\boldsymbol{\varepsilon}}(t)$.

For discretization, we employ a piecewise quadratic DG finite element space on a 60×30 uniform mesh composed of right-angled triangles with a small timestep of $\Delta t = 0.001$ and $N = 50$. During the simulation, our error estimator yields an estimated energy error of $\eta^N = 5.160 \times 10^{-4}$.

Figure 1 illustrates the values of the displacement vectors of the linear elasticity and fractional order viscoelasticity problems at the center of the space domain. In the elasticity problem, we observe an uniform oscillation in the displacement, characteristic of elastic materials, which return to their original shape after the removal of stress, without energy dissipation. In contrast, the viscoelastic case displays a gradual increase in displacement over time due to the memory effect, indicating energy dissipation. As depicted in Figure 2, the elastic material exhibits instantaneous deformation and recovery, whereas the viscoelastic material shows slow deformation and stress relaxation.

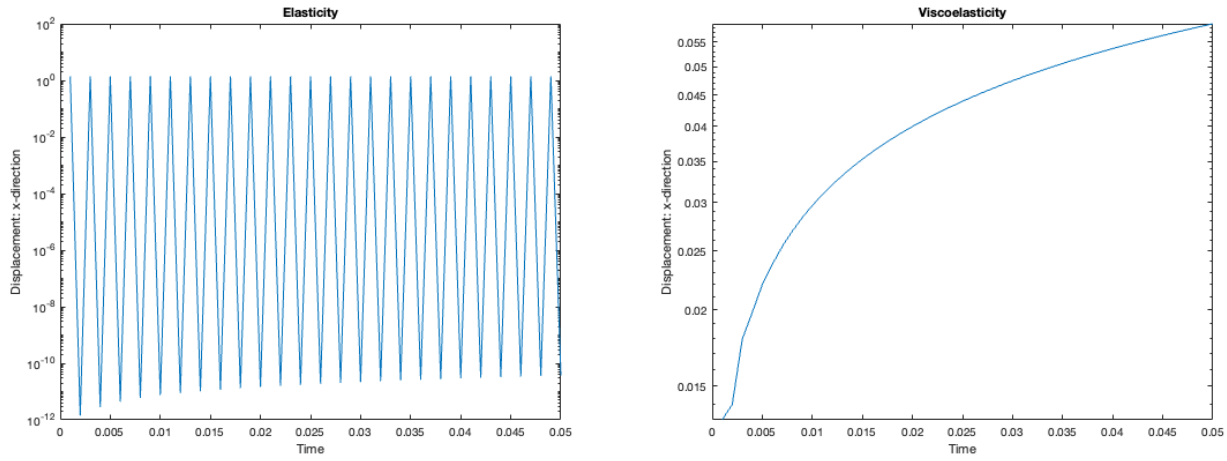

Figure 1: Displacement over time at the center point in the x-direction: the discrete solution $u_1(1, 0.5)$ for the elastic problem (left) and the viscoelastic problem (right).

7 Conclusion

In this study, we developed and analyzed numerical methods for the quasi-static fractional-order viscoelasticity model of power-law type using the symmetric interior penalty Galerkin method. Through the *a priori* error analysis, we demonstrated the stability and convergence of the proposed method, achieving optimal spatial and second-order temporal accuracy. Moreover, we provided the residual-based energy error estimator suitable for complex boundary conditions. Numerical experiments validated the theoretical results, exhibiting the reliability of the error estimator. Furthermore, we compared mechanical responses between elasticity and viscoelasticity, highlighting the importance of fractional-order models in capturing time-dependent behavior. These results contribute to a deeper understanding of viscoelastic materials and provide a robust numerical framework for future research in engineering, material science, and structural analysis.

While our work does not include adaptive algorithms, we can extend our analyses to adaptive hp-DG methods for the model problem with minimal additional effort. Temporal residual error estimates, though not presented here due to space limitations, can be derived using a combination of the Ritz-Volterra reconstruction and Crank-Nicolson reconstruction. These topics are planned for further investigation in our future research.

Conflict of interest

The author declares that there is no conflict of interest.

Data availability

All codes and scripts to reproduce can be found at Jang's GitHub `https://github.com/Yongseok7717/quasi_visco_frac_dg`.

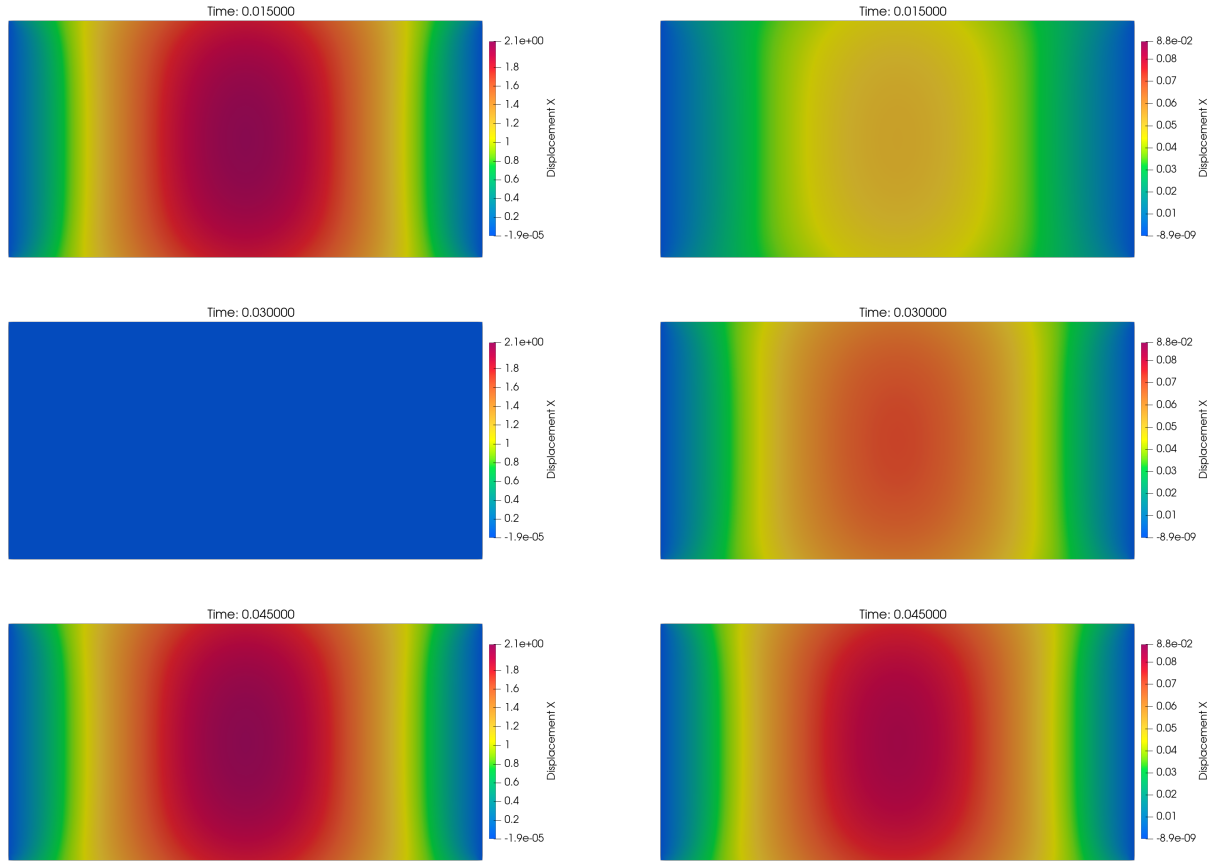

Figure 2: Snapshots of displacement in the x-direction: the discrete solution u_1 for the linear elastic problem (left) and the viscoelastic problem (right) at $t = 0.015$ (top), $t = 0.030$ (middle), and $t = 0.045$ (bottom).

References

[1] S. C. Hunter, Mechanics of continuous media, Halsted Press, 1976.

[2] R. M. Christensen, Theory of viscoelasticity: an introduction, Academic Press, Inc. (London) Ltd., 1971.

[3] J. D. Ferry, Viscoelastic properties of polymers, John Wiley and Sons Inc., 1970.

[4] S. Shaw, J. Whiteman, Some partial differential Volterra equation problems arising in viscoelasticity, in: Proceedings of Equadiff, Vol. 9, 1998, pp. 183–200.

[5] A. D. Drozdov, Viscoelastic structures: mechanics of growth and aging, Academic Press, 1998.

[6] J. M. Golden, G. A. Graham, Boundary value problems in linear viscoelasticity, Springer Science & Business Media, 2013.

[7] P. J. Torvik, R. L. Bagley, On the appearance of the fractional derivative in the behavior of real materials, Journal of Applied Mechanics 51 (2) (1984) 294–298.

[8] W. McLean, V. Thomée, Numerical solution of an evolution equation with a positive-type memory term, The ANZIAM Journal 35 (1) (1993) 23–70.

[9] W. McLean, V. Thomée, Numerical solution via Laplace transforms of a fractional order evolution equation, The Journal of Integral Equations and Applications (2010) 57–94.

[10] W. McLean, V. Thomée, Maximum-norm error analysis of a numerical solution via Laplace transformation and quadrature of a fractional-order evolution equation, IMA journal of numerical analysis 30 (1) (2010) 208–230.

[11] Y. Jang, S. Shaw, A priori error analysis for a finite element approximation of dynamic viscoelasticity problems involving a fractional order integro-differential constitutive law, Advances in Computational Mathematics 47 (3) (2021) 46.

[12] Y. Jang, S. Shaw, Discontinuous Galerkin finite element method for dynamic viscoelasticity models of power-law type, Numerical Methods for Partial Differential Equations 40 (6) (2024) e23107.

[13] S. Larsson, F. Saedpanah, The continuous Galerkin method for an integro-differential equation modeling dynamic fractional order viscoelasticity, IMA journal of numerical analysis 30 (4) (2010) 964–986.

[14] S. Larsson, M. Racheva, F. Saedpanah, Discontinuous Galerkin method for an integro-differential equation modeling dynamic fractional order viscoelasticity, Computer Methods in Applied Mechanics and Engineering 283 (2015) 196–209.

[15] F. Saedpanah, Existence and convergence of Galerkin approximation for second order hyperbolic equations with memory term, Numerical Methods for Partial Differential Equations 32 (2) (2016) 548–563.

[16] S. Shaw, J. R. Whiteman, Numerical solution of linear quasistatic hereditary viscoelasticity problems, SIAM journal on numerical analysis 38 (1) (2000) 80–97.

[17] S. Shaw, J. Whiteman, A posteriori error estimates for space–time finite element approximation of quasistatic hereditary linear viscoelasticity problems, Computer methods in applied mechanics and engineering 193 (52) (2004) 5551–5572.

[18] K. Adolfsson, M. Enelund, S. Larsson, Space-time discretization of an integro-differential equation modeling quasi-static fractional-order viscoelasticity, Journal of Vibration and Control 14 (9-10) (2008) 1631–1649.

[19] J. Fernández, D. Santamarina, An a posteriori error analysis for dynamic viscoelastic problems, ESAIM: Mathematical Modelling and Numerical Analysis 45 (5) (2011) 925–945.

[20] P. Houston, D. Schötzau, T. P. Wihler, An hp-adaptive mixed discontinuous Galerkin FEM for nearly incompressible linear elasticity, Computer methods in applied mechanics and engineering 195 (25-28) (2006) 3224–3246.

[21] R. E. Bird, W. M. Coombs, S. Giani, A posteriori discontinuous Galerkin error estimator for linear elasticity, Applied Mathematics and computation 344 (2019) 78–96.

[22] C. Li, A. Chen, J. Ye, Numerical approaches to fractional calculus and fractional ordinary differential equation, Journal of Computational Physics 230 (9) (2011) 3352–3368.

[23] Y. Yan, M. Khan, N. J. Ford, An analysis of the modified L1 scheme for time-fractional partial differential equations with nonsmooth data, SIAM Journal on Numerical Analysis 56 (1) (2018) 210–227.

[24] L. Banjai, C. Makridakis, A posteriori error analysis for approximations of time-fractional subdiffusion problems, Mathematics of Computation 91 (336) (2022) 1711–1737.

[25] K. Adolfsson, M. Enelund, P. Olsson, On the fractional order model of viscoelasticity, Mechanics of Time-dependent materials 9 (1) (2005) 15–34.

[26] B. Rivière, Discontinuous Galerkin methods for solving elliptic and parabolic equations: theory and implementation, SIAM, 2008.

[27] T. Warburton, J. Hesthaven, On the constants in hp-finite element trace inverse inequalities, Computer Methods in Applied Mechanics and Engineering 192 (25) (2003) 2765 – 2773.

[28] S. C. Brenner, Poincaré–Friedrichs inequalities for piecewise H^1 functions, SIAM Journal on Numerical Analysis 41 (1) (2003) 306–324.

[29] S. Ozisik, B. Riviere, T. Warburton, On the constants in inverse inequalities in L_2, Tech. rep., Rice University (2010).

[30] M. Caputo, Linear models of dissipation whose Q is almost frequency independent—II, Geophysical journal international 13 (5) (1967) 529–539.

[31] K. Oldham, J. Spanier, The fractional calculus theory and applications of differentiation and integration to arbitrary order, Vol. 111, Elsevier, 1974.

[32] E. C. d. Oliveira, J. Machado, A review of definitions for fractional derivatives and integral, Mathematical Problems in Engineering 2014 (2014) 1–7.

[33] S. Shaw, J. Whiteman, Numerical solution of linear quasistatic hereditary viscoelasticity problems ii: a posteriori estimates, Tech. rep., BICOM Technical Report (1998).

[34] Y. Jang, Spatially continuous and discontinuous Galerkin finite element approximations for dynamic viscoelastic problems, Ph.D. thesis, Brunel University London, BURA http://bura.brunel.ac.uk/handle/2438/21084 (2020).

[35] B. Rivière, S. Shaw, J. Whiteman, Discontinuous Galerkin finite element methods for dynamic linear solid viscoelasticity problems, Numerical Methods for Partial Differential Equations 23 (5) (2007) 1149–1166.

[36] Y. Jang, S. Shaw, A priori analysis of a symmetric interior penalty discontinuous Galerkin finite element method for a dynamic linear viscoelasticity model, Computational Methods in Applied Mathematics 23 (3) (2023) 647–669.

[37] S. C. Brenner, Korn's inequalities for piecewise H^1 vector fields, Mathematics of Computation (2004) 1067–1087.

[38] B. Riviere, S. Shaw, J. Whiteman, Discontinuous Galerkin finite element methods for dynamic linear solid viscoelasticity problems, Numerical Methods for Partial Differential Equations: An International Journal 23 (5) (2007) 1149–1166.

[39] B. Riviére, S. Shaw, M. F. Wheeler, J. R. Whiteman, Discontinuous Galerkin finite element methods for linear elasticity and quasistatic linear viscoelasticity, Numerische Mathematik 95 (2) (2003) 347–376.

[40] T. Wihler, Locking-free adaptive discontinuous Galerkin FEM for linear elasticity problems, Mathematics of computation 75 (255) (2006) 1087–1102.

[41] E. H. Georgoulis, O. Lakkis, J. M. Virtanen, A posteriori error control for discontinuous Galerkin methods for parabolic problems, SIAM journal on numerical analysis 49 (2) (2011) 427–458.

[42] O. A. Karakashian, F. Pascal, Convergence of adaptive discontinuous Galerkin approximations of second-order elliptic problems, SIAM Journal on Numerical Analysis 45 (2) (2007) 641–665.

[43] J. M. Melenk, hp-interpolation of nonsmooth functions and an application to hp-a posteriori error estimation, SIAM journal on numerical analysis 43 (1) (2005) 127–155.

[44] P. Ciarlet, Analysis of the Scott–Zhang interpolation in the fractional order Sobolev spaces, Journal of Numerical Mathematics 21 (3) (2013) 173–180.

[45] O. Lakkis, C. Makridakis, Elliptic reconstruction and a posteriori error estimates for fully discrete linear parabolic problems, Mathematics of computation 75 (256) (2006) 1627–1658.

[46] G. M. M. Reddy, R. K. Sinha, Ritz–Volterra reconstructions and a posteriori error analysis of finite element method for parabolic integro-differential equations, IMA Journal of Numerical Analysis 35 (1) (2015) 341–371.

[47] G. M. M. Reddy, Fully discrete a posteriori error estimates for parabolic integro-differential equations using the two-step backward differentiation formula, BIT Numerical Mathematics 62 (1) (2022) 251–277.

[48] G. Akrivis, C. Makridakis, R. Nochetto, A posteriori error estimates for the Crank–Nicolson method for parabolic equations, Mathematics of computation 75 (254) (2006) 511–531.

[49] R. L. Bagley, P. Torvik, A theoretical basis for the application of fractional calculus to viscoelasticity, Journal of Rheology 27 (3) (1983) 201–210.